Response to Reviewer #1
########################

Dear Reviewer #1,

Thanks very much for your comments and suggestions, which we have generally adopted. Our responses to the major and minor comments follow below with your original comments marked by leading ">" characters. In our responses, line numbers denoted as "Lxxx" refer to the original document and "DLxxx" refer to the marked-up version of the new document.

> This is a clearly written and carefully presented manuscript describing an
> optimal estimation retrieval of snowfall from W-band radar reflectivity and
> the associated uncertainties. In particular, the very neat description of the
> optimal estimation framework and of the separation of the different factors
> contributing to the uncertainty of the retrieval makes it a very good
> introductory paper on optimal estimation applied to snow retrieval. Overall,
> the research is sound, but I have two major concerns and few minor comments. I
> recommend the paper for publication after these points are addressed.

> Major comments:

> 1) I think that the conclusions about the overall performances of the
> retrieval for the whole C3VP field campaign is misleading and should be toned
> down. The retrieval presented in this paper requires assumptions on the snow
> particle properties that were obtained in Wood et al. (2015) by exploiting (at
> least partly) the same dataset. On one hand, I can accept that the
> observations used for deriving the properties of the snow particle
> "microphysical model" (mass-size and area-size parameters) can be considered
> as independent since the in-situ observations were combined with X-band radar
> measurements. On the other hand, the particle "scattering model" has been
> specifically selected to get the best match between W-band radar measurements
> and reflectivity computed from in-situ observations. It is therefore not
> surprising that the retrieval of the current paper provides an accumulated
> snowfall in such a good agreement with in-situ data. Therefore, I suspect that
> this impressive agreement is more due to a compensation of errors between the
> different snowfall cases than a very accurate performance of the retrieval as
> the instantaneous errors suggest. I have serious doubts that the same overall
> accuracy could be obtained when using a fully independent dataset. In the
> current version of the paper, a reader could really wonder why we would need
> more accurate observations of snow.

Thanks for this feedback. It seems likely that in this comment "overall performances" refers principally to our description of the agreement of retrieved and observed precipitation rates (e. g., Figure 8 of the revised document) and of the agreement in seasonal accumulation achieved by the retrieval in comparison to that obtained from measured values. We have extended the statement at the end of Section 4, paragraph 1 to elaborate on the C3VP data’s roles in the development of the microphysical and scattering models. Further, we have added a statement near the beginning of Section 4, paragraph 4 indicating that the agreement of observed and retrieved snowfall rates is not unexpected. A similar statement regarding the accumulation comparisons has been added near the beginning of section 4, paragraph 5. Finally, we reiterated this point in paragraph 2 of section 5 (Discussion and conclusions). See DL320, DL337, DL350, DL437.

Other principal results discussed in section 5 include the instantaneous retrieval uncertainties and sources of uncertainties in the retrieved state (paragraph 3), information content (paragraph 4), sources of model-measurement uncetainties (paragraph 5). These results depend mostly on the estimates of observation and forward model uncertainties plus forward model sensititivies and would be at most only weakly sensitive to the concerns raised by the reviewer.

We would appreciate further feedback if these modifications do not target the particular issue intended by the reviewer.

> 2) There is no question about the value of the optimal estimation retrieval
> described in this paper, in particular for assessing the different
> contributors to uncertainty. However, since the retrieval is applied to a
> single radar range gate and attenuation is neglected, and based on the
> conclusion that the W-band reflectivity is much more sensitive to log(lambda)
> than log(N0), it sounds that a much simpler retrieval (such as Z-lambda
> statistical relation) could be proposed with performances probably similar the
> optimal estimation proposed in this study. Please comment.

One of the benefits of this retrieval approach is that the retrieval can, on-the-fly, determine appropriate weights to apply to the information in the observations versus information provided by the a priori. Since Z alone cannot uniqely determine S, a priori information of some form is required. For simple statistical retrievals, this a priori information is generally embedded in the statistical relationships. It's not clear to us that this information-based weighting would be provided in a simple statistical retrieval.

That said, simple temperature-dependent statistical relationships that would provide estimates of snowfall rate and their uncertainties could be constructed. See, for example, Figure 7 of the revised manuscript to see how Z-S for this retrieval varies with temperature. There are some drawbacks:

First the differences in sensitivity and information that are made explicit with this method tell us quantitatively that a Z-lambda approach would not be sufficient. It's clear that the retrieval requires information about N0 that is not provided well by the Z measurement, so a priori information about N0 is required. Diagnostics like this would not be obtainable in a simple statistical retrieval.

Second, consider what must be done when observed snowfall rate values are found to depart substantially from the retrieved values (i.e., the retrieval fails). With this method it's straightforward to compare the retrieval's assumptions, which are explicit, against observations to determine the cause of the retrieval failure. With a statistical approach, in which the a priori assumptions are typically not explicit, the causes of retrieval failure are much less transparent.

> Minor comments:

> 1) L145: In order to emphasize that observations are independent, I would
> specify that X-band radar observations were used in Wood et al. (2015) for
> deriving the snow particle "microphysical model".

1) Done. We have revised the referenced sentence (in the first paragraph of section 2.1.1, in the text following equation 8) to read "That work used in-situ measurements and remotely-sensed X-band reflectivity observation of snow from C3VP...". (DL151)

> 2) L300-303: Related to my major comment, by checking Wood et al. (2015), it
> appears that the 3 cases mentioned were indeed used for deriving the snow
> particle "microphysical model". However, practically the same overall dataset
> (Wood et al. (2015) say: "13 days from 2 December 2006 to 26 February 2007")

> was used to select the particle "scattering model".

2) Yes, this is correct. The microphysical properties (m(D) and A(D)) and generic shape (which with m(D) and A(D) determine the scattering properties) used different ranges of the C3VP observations owing to differences in the availability of the required observations.

In W15, first, observations from 4 snowfall events were used to estimate the PDFs of microphysical properties (m(D) and A(D) but not shape). The data described in Table 1 of this manuscript for 6-7 December 2006 and 26-27 January 2007 are from small time periods of three of these events (SYN1, LE1, and LE2) during which the ACR was operated. Second, given m(D) and A(D), particles of different generic shapes or habits were modeled and radar scattering properties were calculated. ACR observations from the "13 days from 2 December 2006 to 26 February 2007" were then used to determine the generic shape that best reproduced the observed reflectivities. See our response to major comment #1.

> 3) Table 1: While I was trying to understand which part of the C3VP dataset
> was used for each part of the work in the current study and in Wood et al.
> (2015), I realized that the 3 common cases reported both in Wood et al. (2015)
> and in the current study don't show the same FD12P snow accumulation in LWE mm
> (0.8 vs 3.2 mm for the 6 Dec. 2006 ; 0.093 vs 10.2 mm for the 7 Dec. 2006 and
> 1.06 vs 4.6 mm for 27 Jan. 2007). These numbers are very different, please
> clarify. The accumulation is always smaller in the current paper. If the data
> on those days was only partially used, please explain why.

3. While the FD12P and other instruments involved in the study were mostly autonomous and ran continuously during snowfall events, the ACR required an attending operator and so ran for shorter periods of time within the events. Note that the durations shown in Table 1 are substantially shorter than those shown for the events used in W15.

> 4) L381-388: It would help the understanding if you introduce the sensitivity
> of the forward model to both log(lambda) and log(N0) at the same time while
> saying that the sensitivity to N0 is not shown in a figure because it is
> constant and equal to 10.

4. We have revised the paragraph (3rd paragraph of section 4.2, near line 405 of the revised manuscript) to introduce earlier the constant sensitivity to log(N0) in contrast to the varying sensitivity to log(lambda). (DL412)
Typos and awkward phrasing:

1) L57: evaluate is used twice

The second instance of "evaluating" has been changed to "estimating".

2) L125: "based on information theory"

"based in" is our intended wording.

3) L191: "Northwest"

"Northewest" has been corrected. (DL197)

4) L276: missing number after comma?

To clarify, we have written this as "0.00", which is the actual value to two decimal places. (DL287)

> 5) L444: reduce is used twice

"reduced by reducing" is our intended wording.

Response to Reviewer #2
#######################

Dear Dr. Maahn,

Thank you very much, we appreciate your comments and suggestions. Our responses to your general and specific comments follow with your original comments marked with leading ">" characters. In our responses, line numbers denoted as "Lxxx" refer to the original document and "DLxxx" refer to the marked-up version of the new document.

> The authors present a snowfall retrieval based on radar reflectivity and
> temperature. While similar retrievals have been developed before, the focus
> of using only a single radar reflectivity and the extraordinary detailed error
> analysis makes it nevertheless an important contribution. The paper is well
> written, shows attention to detail, and the figures are clear. I have quite a
> few comments, but they are all of minor importance and I recommend the paper
> to be published subject to the following comments:
>
> Does this paper describe how CloudSat's 2C-SNOW-PROFILE works? If yes, I
> would recommend to say so. If not, I would recommend to mention the
> differences

Yes, with the exception that the retrieval here operates on single-range-bin reflectivity observations (and for this analysis involves no treatments for attenuation, multiple scattering or spatial correlation), this is the retrieval method used for CloudSat's 2C-SNOW-PROFILE. A companion paper is near completion - it extends this retrieval to CloudSat Cloud Profiling Radar observations. We have added a statement indicating the relationship to the CloudSat retrieval in the introduction. (DL76)

> I wonder how does this retrieval compares to traditional Ze-P relations?
> Clearly the sophisticated error estimates are an advantage, but what about the
> absolute P values? For several fixed temperature values, can the authors plot
> P as a function of Ze? This would allow to see 1) where the retrieval deviates
> from a power law form, 2) the impact of temperature on P, and 3) how it
> compares to published Ze-P relations

Yes, we've prepared a figure that shows the temperature dependence of the Z-S results obtained for this retrieval and makes comparisons of our results against a number of published Z-S relationships. It is included as Figure 7 in section 4 of the revised manuscript. Our results are consistent with several of these relationships at reflectivities up to about 5-7 dBZe. Above 7 dBZe, our results tend toward smaller snowfall values than a purely linear relationship would produce. The smaller values are more consistent with the Kulie and Bennartz (2009) HA particle results, which represent an aggregate particle. For our results, snowfall rates at a given Z become larger generally with warming temperature.

> Specific comments

> L120: I assume the authors refer to the a posteriori covariance of x?

Yes, it is the current, iterative estimate of the a posteriori covariance of x, exactly. We have reworded the description to provide this information. (DL124)

> L124: Is this the test shown in chapter 12.3.2 of Rodgers, 2000?

Yes, This test is actually obtained from Marks and Rodgers (1993) from their equation (16) and the discussion that follows, but it is the implementation of the test for correct convergence described by Rodgers (2000) in section

12.3.2. We now also include a citation of Marks and Rodgers. (DL129)

> L169: Do the authors underestimate Dmax when they use a measurement by an
> optical instrument? Isn't is quite unlikely that an individual particle is
> rotated such that the true Dmax can be observed?

The optical instruments do underestimate Dmax (see Wood et al., 2013, for example). The retrieval used in Wood et al. (2015) to determine the microphysical and scattering a priori properties used in this retrieval includes compensation for this effect. Accordingly, the particle a priori properties used in this retrieval are based on Dmax and so the retrieved size distribution parameters are those for Dmax.

> L174: does the log(N0) distribution have a Gaussian shape?

Yes, much more so that would N0 itself. Please see the figure N0_Dmax_histograms_SVI_C3VP.png we provided with our online discussion comments.

> L204: Do the authors think that their results are also applicable to high
> latitude locations?

Yes, although that opinion is based on tests done with the actual CloudSat retrieval product in comparisons against ground-based observations (primarily in Antarctica and Sweden). Please see for example Lemmonier et al., 2020, doi:10.1029/2019JD031399.

> Figure 1) Why is the aircraft based N0 higher than the ground-based? Has the
> C3VP dataset been corrected for in situ probe shattering effects?

The differences appear more substantial than what would be attributable to shattering (this is based on a quick look at the corrected versus uncorrected distributions in Field et al., 2006, JTECH). The aircraft data in Figure 1 include observations well above the surface. We expect that the differences are largely due to microphysical processing between locations aloft and the surface. Unfortunately, documentation for the C3VP aircraft 2D probe particle data do not indicate whether shattered particle correction was performed.

> L228: Typo in SF

Corrected, thank you. (DL234)

> L233: I would say that Optimal Estimation cannot handle biases at all. I
> think it is perfectly acceptable that the authors assume that the CPR does not
> have any bias, but I would recommend to remove 'uncertainty in the absolute
> radiometric calibration'

We agree, but we've revised this sentence somewhat differently than suggested. We indicate that both bias and measurement noise contribute to reflectivity errors, but that we've used the CPR noise characteristics to estimate S_y. (DL239, 241)

> L247: Defining Kb is a very important step, I would recommend to spend 2-3
> sentences on it instead of referring only to previous work.

This paragraph was revised to provide more details about K_b. (DL252)

> Figure 3: Add to the caption that measurement uncertainty is shown.

Done, the caption was changed to indicate that measurement uncertainty is shown. (Near DL256)

> L266: I appreciate that the authors do handle the errors sources
> conservatively and do not oversell the retrieval's uncertainty, but I wonder
> whether they are a little bit too pessimistic here: A radar always observes
> thousands of particles, isn't it quite unlikely that they are all of the same
> kind? Maybe a more recent bulk scattering method such as SSRGA would work
> better?

Another way to look at this question is to ask, given two different radar volumes filled with particles that follow exactly the same m(D), same Ap(D) and same size distribution but whose particle shapes are not constrained to match each other, does it seems reasonable that their reflectivities could differ by about 2 dB? That seems possible, but yes, may be conservative especially given that, for snowfall, we are often observing populations of irregular aggregates rather than pristine particles..

> L281: Why didn't the authors use the follow up paper by Heymsfield and
> Westbrook (2010)?

There was no strong reason for not using Heysfield and Westbrook (2010) for fallspeeds. As part of other work (described in Wood et al., 2014, 2015), we performed tests by switching between HW2010 and Mitchell and Heymsfield (2005) and found little impact on those retrieval results, but we should revisit our choice for this retrieval.

> L286: I would recommend to provide some details about S_b, I guess it
> contains the uncertainties of the m(D) relation?

We have revised equation 19 slightly to clarify that S_{\tilde{b}} is the uncertainty in snowfall rate that results from the uncertainties in the particle model parameters, and added a description of how it is calculated. (DL301)

> Figure 8: A more convincing evaluation example would be to use a different
> data set, e.g. from the high Arctic

We agree there would be value in comparing against other datasets, but this comparison does illustrate the effects of substantial departures from the a priori assumptions of the retrieval and the behavior of accumulation errors. We do plan to apply this retrieval method to other field experiment datasets that involve ground-based radars.

> L345: I wonder whether the discussion about accumulation errors is relevant
> for CloudSat since it can provide only a snapshot of the current measurements?

We are examining the calculation of accumulations from intermittent observations (such as provided by CloudSat) and the resulting errors for the companion paper. We agree, it isn't clear that the treatment here for a fixed radar taking essentially continuous meausrements would be highly applicable to CloudSat.

> L376: Why is the number of states 0.9 higher than H?

It's a bit of a numerical coincidence due to the particular values of H. The number of states is given by 2**H (described well in the L'Ecuyer et al., 2006 reference).

> L378: A couple of years ago, I had the same problem and, after thinking
> about it a long time and checking my code many times, came to the same
> conclusion, i.e. it is related to high correlations. However, I looked into
> the same issue recently and found that the negative values on the diagonal of
> A disappear after I added checks making sure that my covariance matrices are
> not singular: Python's (and I guess this applies to other languages, too)
> built-in inversion routine is quite forgiving and also inverts matrices that
> are 'slightly' singular. However, these instabilities can add up and many
> matrix inversions later lead to a negative entry on the diagonal of A. And it
> turned out I had created the singular matrix by myself by applying the
> authors' eq. 16 which added some numerical noise making my S_Epsilon singular
> and non-symmetric. After making sure that my S_Epsilon is really symmetric and
> nonsingular (i.e. doing a rank test), negative values on the diagonal of A
> disappeared. I admit I never investigated this systematically, so it could be
> a coincidence, but I would be curious to see whether the authors' negative
> values are also related to numerical instabilities. In the end, this appears
> to be a cosmetic issue and not very important: the total degrees of freedom
> and all other results stayed the same in my sample retrieval.

Thanks very much for providing this information. In this single-bin reflectivity-only retrieval, the S_Epsilon matrix consists of a single element, so is never ill-conditioned. The other matrix that must be inverted and that is used in the A-matrix calculation is the a priori covariance, S_a; its condition number is around 20. The final matrix that must be inverted has condition numbers ranging from 35 to 95. These are somewhat large, but indicate a potential loss of precision of only 1-2 decimal places in the inverse calculation (which uses double-precision arithmetic). Based on these values, we think it seems less likely that ill-conditioning is the source of the negative A-matrix values.

> Figure 12: I'm surprised that the d_s values are not higher. A couple years
> ago I developed an ice cloud retrieval where I, because it was an information
> content study, simply added everything to the state vector: 3 PSD parameters,
> 2 m(D) parameters, and 2 A(D) parameters. With such a large state vector, I
> always got two d_s when using Ze and mean Doppler (I never tried only Ze). The
> fact that d_s is not 1 in the authors' study might mean that a little bit of
> information is unused. I wonder whether this information could be used and d_s
> would be 1 if the m(D) parameters were moved from the b vector to the x
> vector. This might lead to lower P uncertainties. This would also help with
> the issue raised in L419. Of course, this includes the challenge to make sure
> that the retrieval doesn't put all the information into m(D) instead of the
> PSD parameters which probably would make the P uncertainty even larger.

This is an interesting interpretation. Yes, it seems it could be an indication that the retrieval is prevented from fully utilizing the information in the reflectivity observation. It would be interesting to try including m(D) parameters in the state vector. This would require the forward model to update particle scattering properties as m(D) parameters are adjusted, so a less computationally-intensive method (compared to DDA) would need to be used to calculate those properties - perhaps the SSRGA approach you mentioned earlier.

> L450: Add the DOI

At this time, the effort by the GHRC to archive the C3VP observations (including those used in this study) was initiated as a result of this manuscript and is not complete. We are looking at alternate archive locations and will need to add the necessary information prior to final publication. We have added a placeholder data availability statement. (DL535)

> Heymsfield, A. J., and C. D. Westbrook, 2010: Advances in the Estimation of
> Ice Particle Fall Speeds Using Laboratory and Field Measurements. J. Atmos.
> Sci., 67, 2469-2482, doi:10.1175/2010JAS3379.1.

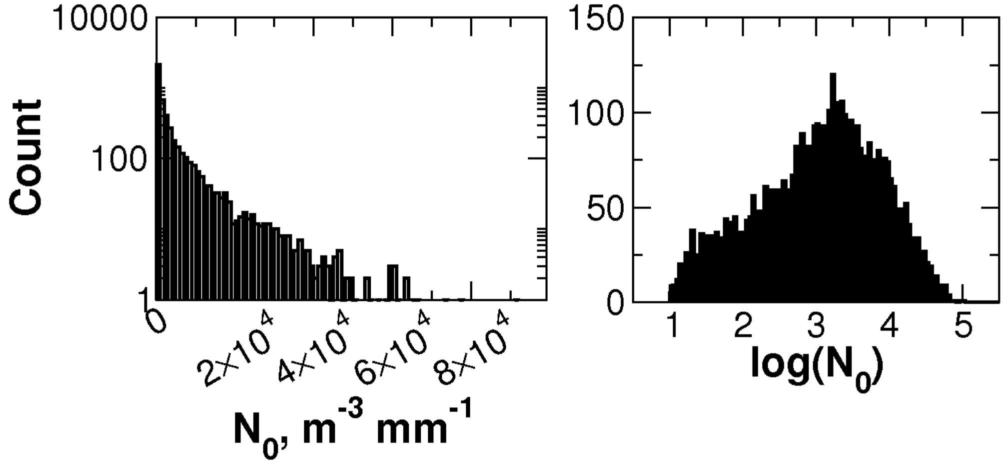

Figure 1: N0_Dmax_histograms_SVI_C3VP.png

Response to Reviewer #3
#######################

Dear Reviewer #3,

Thank you for your feedback and requests for clarification. Our responses to your comments follow below with your original comments marked with leading ">" characters. in our responses, line numbers denoted as "Lxxx" refer to the original document and "DLxxx" refer to the marked-up version of the new document.

> This manuscript describes the optimal retrieval process for deriving snowfall
> from single millimeter-wavelength radar reflectivity observations and
> represents a derived uncertainty analysis divided into the relevant error
> sources in the process. The manuscript is logically and well structured, and
> fluently written. The topic has been walked through by describing the steps
> nicely and in an informative way, and the manuscript was very nice to read.
> Although the topic is not necessarily very novel, when more recently the
> tendency has been on describing the multi-frequency retrieval processes or
> retrievals combining single-frequency with Doppler-velocity information, the
> way the authors describe the details in the process, and especially, the
> factors influencing the uncertainty, the manuscript has a significant
> contribution and is relevant and interesting for the community. My
> recommendation is that the manuscript should be published with minor changes
> and clarifications.

> Below I have a few small requests for clarifications for the authors.

> Request for clarification:

> 1. My major concern in the development of the retrieval process is that it is,
> if I have understood correctly, based on almost single simplified snow model
> (Wood et al.2015) with single values of (alpha, beta, gamma, sigma) with a
> certain uncertainty stated in Appendix B. Although, it has been shown e.g. in
> Kulie and Bennartz, 2009 in Figure 1, the huge variety in backscattering
> coefficients for different particle types and as it is stated also in the
> manuscript e.g. on line 246 that in Wood et al. 2015 the uncertainties for the
> described perturbed particle models can be as high as 15 dB. What about the
> effect of aggregation creating very different particle properties (low area
> ratio) from single crystals or rimed particles? I wonder could this be the
> reason for the two outlier cases described in the results in paragraph
> starting on line 319 that the particle types (m(D) and v(D) were so different
> from the used parametrization of Mitchel and Heymsfield 2005), and the used
> particle model were not descriptive for the observed particles, although still
> dry snow particles and not e.g. melting as proposed in the manuscript on line
> 403. And therefore, the retrieval failed. Actually, looking at the Figure 7
> with all higher snowfall rates (> 0.8 mm), the retrieval seems to
> underestimate quite systematically. If seen also as relevant, could the
> authors provide more discussion on this topic to the manuscript although there
> is already the statement on line 403?

Yes, aggregation could lead to dry snow particles with properties that are very different from those used as a priori assumptions in the retrieval. In general, aggregation (and other microphysical processes) may change how mass, area, fallspeed, and scattering properties all vary with particle size D. The retrieval has some freedom to adapt to this by altering the retrieved log(lambda) and log(N0) so that the forward-modeled Ze matches the observed Ze. Large differences, however, will likely lead to nontrivial retrieval errors.

For the 14 February anomaly, in addition to the evidence mentioned briefly in the manuscript, a collocated X-band Doppler radar (McGill University's VertiX) revealed a bright band at around 1 km AGL with Doppler velocities of around 3 m/s below this level. This is a large fallspeed for dry snow aggregates, but these might have been large, wet aggregates. The VertiX was not in operation for the 2 March anomaly. It's probably not possible to rule out that aggregation was involved in either anomaly.

Yes, there does seem to be underestimation for higher snowfall rates in Figure 7 (now Figure 8), balanced by overestimation to some degree as evidenced by events with positive fractional differences in accumulations shown in Table 1. This suggest there might be a benefit for making the particle model a function of the observed reflectivity, and should be investigated further.

We have revised the statement in the Discussion section (DL439) to be more consistent with this clarification.

We have also added brief commentary in the 4th paragraph of section 4 (DL345).

> 2. As a second point, in my understanding, the Z-S retrieval is less dependent
> on the intercept parameter in the millimeter wavelength than in the centimeter
> region where the Rayleigh approximation is applicable (e.g. Rasmussen et al.
> 2003, BukovcÌ\214icÌ\201 et al. 2018). In the abstract, it is stated on line 14, that
> the PSD intercept is less well constrained by the retrieval, and in Appendix
> on line 488, that the measurements better sensitive to log(N0) could benefit
> the retrieval. Could the authors elaborate, whether hese results refer that
> the dependence on N0 is physically no longer similar significant to the
> retrieval.

Yes, log(N0) is still physically significant to the retrieval, since it does influence Ze and snowfall rate; however log(lambda) is more strongly constrained by the reflectivity measurement than is log(N0). That means that the retrieval must employ either "a priori" information or additional measurements to help constrain log(N0).

> And continuing, would then actually simple averaged Z-S relations provide
> equally good retrieval results, in case the particle type and shape are
> correctly modeled? The retrieval results here are compared to the collocated
> measurements of accumulation with a weather sensor. It would be also
> interesting to see, how different are the snowfall rates with this presented
> optimal retrieval method in comparison to these simple Z-S relations presented
> in the literature such as e.g. Kulie and Bennartz, 2009 or Matrosov, 2007.

Regarding simple, averaged Z-S relationships, please see Figure 7 that has been added to the manuscript. The retrieval gives Z-S relationships that are temperature-dependent and that deviate from the plotted linear relationships obtained from published Z-S relationships. It seems likely that temperature-dependent functions could be developed that mimic the Z-S behavior of the retrieval (but not the information-centric diagnostics). Please see also our response to reviewer #1.

> Small comments:

> In the paragraph starting on line 29, the ground-based radar observations are
> described. It is slightly striking that only MRR related literature references
> are stated, even though this paper is describing the retrieval process
> utilized for the W-band. Was there a certain reason for this choice, why e.g.
> other studies presenting W-band observations were left out? Although, some of
> the radars are mentioned on lines 71-73.

No, there wasn't a conscious decision to omit W-band radars. For experiments like these, W-band radars, because of their primary application as cloud radars, are more often operated for cloud measurement from aircraft and less often for observing snowfall at the ground. We know that GCPEx and ICE-POP in addition to C3VP all deployed ground-based W-band radars. Two Department of Energy funded experiments (StormVEx, at Colorado's Storm Peak Laboratory and BAECC in Finland), also deployed ground-based W-band radars. A number of studies have used W-band radar observations as part of multi-frequency snowfall retrievals, which are not applicable to this work. Development of snowfall retrievals using single-frequency, ground-based radar observations at W-band is not common. Some work has been done using ground-based Ka-band radars for snowfall (e g., Matrosov et al., 2008, JAMC; Cooper et al., 2017)

We have revised the text to include information about experiments with ground-based W-band radars. (DL38)

> Figure 11. Suggestion to use a different color for FD12P to improve
readability.

Done, and symbol sizes were increased to improve clarity. (near DL400)

> Line 381 Suggestion to use a different term for shape of the size
> distributions. Although it is clear that the exponential PSD distribution is
> used here and this term describes the effect of lambda in the metric curves in
> Figure 13, it still is close to the widely used shape parameter Âµ of gamma
> PSD.

We changed this to say simply that "The size distribution plays a significant role..." (DL411)

> Typos:

> Line 307 should be Vaisala FD12P (Vaisala Oyj, 2002) instead of (Viasala Oyj,
> 2002)

"Viasala Oyj" is changed to "Vaisala Oyj". (DL332)

> Line 336 remove the unit

"unit" removed, thanks. (DL366)

> Rasmussen, R., M. Dixon, S. Vasiloff, F. Hage, S. Knight, J. Vivekanandan, and
> M. Xu, 2003: Snow Nowcasting Using a Real-Time Correlation of Radar
> Reflectivity with Snow Gauge Accumulation. J. Appl. Meteor., 42, 20â\200\22336,
> https://doi.org/10.1175/1520C3

> BukovcÌ\214icÌ\201, P., A. Ryzhkov, D. ZrnicÌ\201, and G. Zhang, 2018: Polarimetric Radar
> Relations for Quantification of Snow Based on Disdrometer Data. J. Appl.
> Meteor. Climatol., 57, 103â\200\223120, https://doi.org/10.1175/JAMC-D-17-0090.1.

> Kulie, M. S., and R. Bennartz, 2009: Utilizing spaceborne radars to retrieve
> dry snowfall. Journal of Applied Meteorology and Climatology,48 (12),
> 2564â\200\2232580, doi:10.1175/2009JAMC2193.1.

> Matrosov, S. Y., 2007: Modeling backscatter properties of snowfall at
> millimeter wavelengths.619Journal of the Atmospheric Sciences,64 (5),
> 1727â\200\2231736, doi:10.1175/JAS3904.1.

Matrosov, S.Y., M.D. Shupe, and I.V. Djalalova, 2008: Snowfall retrievals using millimeter-wavelength cloud radars. J. Appl. Meteor. Climatol., 46, 769-777. doi:10.1175/2007JAMC1768.1

Cooper S. J., N. B. Wood, and T. S. L'Ecuyer, 2017: A variational technique to estimate snowfall rate from coincident radar, snowflake, and fallspeed observations. Atmos. Meas. Tech., 10, 2557-2571, doi:10.5194/amt-10-2557-2017.

What millimeter-wavelength radar reflectivity reveals about snowfall: An information-centric analysis

Norman B. Wood[1] and Tristan S. L'Ecuyer[2]

[1]Space Science and Engineering Center, University of Wisconsin - Madison, Madison, WI
[2]Department of Atmospheric and Oceanic Sciences, University of Wisconsin - Madison, Madison, WI

Correspondence: Norman B. Wood (norman.wood@ssec.wisc.edu)

Abstract. The ability of single-frequency, millimeter-wavelength radar reflectivity observations to provide useful constraints for retrieval of snow particle size distribution (PSD) parameters, snowfall rates, and snowfall accumulations is examined. An optimal estimation snowfall retrieval that allows analyses of retrieval uncertainties and information content is applied to observations of near-surface W-band reflectivities from multiple snowfall events during the 2006-2007 winter season in southern Ontario. Retrieved instantaneous snowfall rates generally have uncertainties greater than 100%, but single-event and seasonal snow accumulations from the retrieval results match well with ~~independent~~ collocated measurements of accumulations. Absolute fractional differences are mainly below 30% for individual events that have more substantial accumulations and, for the season, 12.6%. Uncertainties in retrieved snowfall rates are driven mainly by uncertainties in the retrieved PSD parameters, followed by uncertainties in particle model parameters and, to a lesser extent, the uncertainties in the fallspeed model. Uncertainties attributable to assuming an exponential distribution are negligible. The results indicate that improvements to PSD and particle model a priori constraints provide the most impactful path forward for reducing uncertainties in retrieved snowfall rates. Information content analyses reveal that PSD slope is well-constrained by the retrieval. Given the sensitivity of PSD slope to microphysical transformations, the results show that such retrievals, when applied to radar reflectivity profiles, could provide information about microphysical transformations in the snowing column. The PSD intercept is less well constrained by the retrieval. While applied to near-surface radar observations in this study, the retrieval is applicable as well to radar observations aloft, such as those provided by profiling ground-based, airborne, and satellite-borne radars under lighter snowfall conditions when attenuation and multiple scattering can be neglected.

1 Introduction

Radar observations focused on snowfall from platforms outside the established weather surveillance radar networks have become ubiquitous over the last two decades, largely due to increased interest in the role of snowfall in mid- and high-latitude microphysics, hydrology and climate. This research accelerated with the advent of satellite-borne radars flown by missions to quantify global hydrometeor and precipitation properties. These satellite-borne radars (specifically the CloudSat mission's Cloud Profiling Radar (CPR) (Tanelli et al., 2008) and the Global Precipitation Measurement (GPM) mission's Dual-frequency Precipitation Radar (DPR) (Toyoshima et al., 2015), with two others anticipated to launch in the coming decade) are capable solely of measuring vertical profiles of radar reflectivity factor (hereafter, reflectivity) along with path integrated attenuation under certain conditions. To understand the capabilities of these satellite-borne radars for quantifying snowfall, we must know how well radar reflectivity observations constrain snowfall properties.

To these ends, CloudSat and GPM have contributed to multiple field experiments involving ground-based radars and designed to provide, in part, ground validation data for the radar remote sensing of snowfall: the Canadian CloudSat-CALIPSO Validation Project (C3VP) (Hudak et al., 2006), the Global Precipitation Measurement (GPM) Cold-season Precipitation Experiment (GCPEx) (Skofronick-Jackson et al., 2015), the Light Precipitation Validation Experiment (LPVEx) (Petersen et al., 2011), the International Collaborative Experiment during the PyeongChang 2018 Olympics and Paralympics (ICE-POP) (Chandrasekar et al., 2019), and the Olympic Mountains Experiment (OLYMPEx) (Houze et al., 2017). ~~Ground-based profiling radars such as the METEK Micro Rain Radar (MRR) (Klugmann et al., 1996), which operates at the transition between millimeter and centimeter wavelengths, have been key components of these larger field experiments. In addition,~~ These and a number of smaller, more focused field campaigns (Pettersen et al., 2020; Schirle et al., 2019) ~~deployed MRRs exclusively for vertically profiling frozen precipitation. While~~ have made extensive use of small K-band profiling radars, e. g, METEK's Micro Rain Radar (MRR, Klugmann et al., 1996), but several experiments, including C3VP, GCPEx and ICE-POP have deployed ground-based, W-band scanning or profiling radars. Although these ground-based radars may provide ~~additional~~ advanced capabilities such as Doppler velocity measurement, their reflectivity measurements in snowfall are a valuable resource for examining the capabilities of the satellite-borne radars ~~(Maahn et al., 2014)~~(Maahn et al., 2014; Matrosov et al., 2008).

The ability of radar reflectivity to constrain snowfall properties, however, has not been well evaluated. Snowfall exhibits a wide range of microphysical characteristics that influence radar reflectivity and snowfall rate. Most notable to casual observers are variations in particle habits: pristine dendrites, needles, columns, plates and bullets; aggregates of the same; pellets and graupel for example. Underlying these differences in habit are variations in mass, and, given a particular mass, variations in how mass is distributed within the particle. Unlike longer-wavelength radars for which radar backscattering properties of snow particles are sensitive primarily to particle mass, at millimeter wavelengths those properties are additionally sensitive to particle shape. Investigations of particle mass and area (an aspect of shape) (Kajikawa, 1972, 1975, 1982; Zikmunda and Vali, 1972, 1977; Heymsfield, 1972; Locatelli and Hobbs, 1974; Mitchell et al., 1990; Mitchell, 1996; Heymsfield and Miloshevich, 2003) have painstakingly determined the broad extent of these variations. Along with differences in single-particle properties, populations of falling snow particles vary substantially in their concentrations with size (i.e., the spectral particle size distribution, PSD) based on measurements from the ground (e.g., Nakada and Terada, 1935; Imai et al., 1955; Gunn and Marshall, 1958; Rogers, 1973; Brandes et al., 2007) and more recently, with the advent of imaging particle probes, from aircraft (e.g., Passarelli, 1978; Gordon and Marwitz, 1984, 1986; Braham, 1990; Woods et al., 2008; Heymsfield et al., 2008, and references therein). The observed particle concentrations vary over several orders of magnitude.

In radar-based remote sensing scenarios when these properties are not known, these variations produce uncertainty in the relationship between radar reflectivity factor (hereafter, reflectivity) and associated water content and snowfall rate. A common approach to ~~evaluating~~ estimating this uncertainty has been to evaluate modeled reflectivities, water contents and snowfall rates using a range of assumed particle models and PSDs. The results are often expressed using relationships between reflectivity and snowfall rate ("Z-S" relationships) (Liu, 2008; Kulie and Bennartz, 2009; Matrosov et al., 2008, 2009). This approach allows the uncertainty in a retrieved snowfall rate to be estimated, but the existing studies have not provided insight into the dominant sources of uncertainty nor into the ability of observed radar reflectivity to constrain various properties controlling the snowfall rate. Posselt et al. (2015) examined uncertainties and information content for radar observations of mixed- and ice-phase regions of a convective storm, but targeted radar systems with more advanced capabilities. Mascio and Mace (2017) used CloudSat and aircraft observations to assess how uncertainties in the ice particle mass-dimension relationship contribute to radar reflectivity forward model uncertainties, but used known, observed particle size distributions and did not examine the influence of the mass-dimension uncertainties on snowfall retrieval performance.

In this work, we provide uncertainty and information content analyses for retrieving snowfall from observations of radar reflectivity at millimeter wavelengths, focusing on W-band (94 GHz). The results are representative of the general problem of estimating snowfall from such remote radar reflectivity observations without supplementary collocated observations of snow particle mass-dimension relationships, fallspeeds, and particle size distributions. The results apply particularly to observations by the CPR (Tanelli et al., 2008) and by the DPR's Ka-band radar, but also to reflectivity measurements from ground-based radars such as the MRR (Klugmann et al., 1996) and the Department of Energy Atmospheric Radiation Measurement (ARM) program's Millimeter Wavelength Cloud Radar (Moran et al., 1998) and Ka-band ARM Zenith Radar (KAZR) (Bharadwaj et al., 2013). ~~Our objectives~~ The retrieval method used here is the foundation for the retrieval used for CloudSat's 2C-SNOW-PROFILE product; that application is the subject of a future companion paper. Our objectives here are to identify the snowfall properties that are best constrained by such observations and the most significant sources of uncertainty in the radar retrieval of snowfall. The results establish a performance baseline for reflectivity-only observations of snowfall, indicate where uncertainty reduction efforts should be focused, and suggest what improvements to radar observing systems could be most beneficial.

The analyses use the optimal estimation (OE) retrieval technique (Rodgers, 2000), which inherently diagnoses information content and uncertainties in retrieved quantities subject to specified uncertainties in measurements, forward models, and a priori knowledge of the quantities to be retrieved (L'Ecuyer et al., 2006; Cooper et al., 2006). The retrieval produces best-estimates of snow size distribution parameters by using the radar reflectivity observations to refine a priori estimates of those parameters (Sect. 2). The information content metrics provided by OE require all sources of uncertainties in the retrieval process to be specified. These are discussed in Sect. 3. Ground-based radar and precipitation observations allow the retrieval to be tested, showing that size distribution width is best constrained by the retrieval and that uncertainties in retrieved size distribution parameters (but not uncertainties due to the assumed exponential form of the PSD itself) are the strongest contributors to uncertainties in estimated snowfall rates (Sect. 4). The results suggest that the retrieved size distribution widths could be useful for diagnosing changes in PSD resulting from microphysical processes (Lo and Passarelli, 1982) and that improved observational constraints on size distribution parameters, as might be provided by dual-wavelength radar observations (Matrosov, 1998), would likely enhance snowfall retrieval performance (Sect. 5).

2 Retrieval method

The retrieval uses measurements of reflectivity to estimate snow microphysical properties and to quantify water content and snowfall rate. At the wavelengths characteristic of cloud radars such as CloudSat and shorter-wavelength precipitation radars, scattering by precipitation-sized particles does not follow the Rayleigh approximation, and both attenuation and multiple scattering may affect the radar signal. At these wavelengths, snow particle scattering and extinction properties depend not only on mass, but on shape as well. With even simple parameterized expressions for particle mass, shape, and size distribution (PSD), single-frequency observations of radar reflectivity alone are insufficient to reasonably constrain the resulting set of parameters.

To address this insufficiency, retrievals must incorporate a priori information about particle microphysical and scattering properties. This is accomplished here using OE (Rodgers, 2000), a Bayesian technique that allows a priori information to be included explicitly. The input for this retrieval is the Z_e observed by the radar for a range gate identified as containing snow. For notational consistency with other work, we show this as a vector:

$$\boldsymbol{y} = \left[Z_{e,1}^{obs}\right]. \tag{1}$$

A forward model $\boldsymbol{F}(\boldsymbol{x},\tilde{\boldsymbol{b}})$ relates $\boldsymbol{y}$ to $\boldsymbol{x}$, a state vector of unknown properties to be retrieved, as

$$\boldsymbol{y} = \boldsymbol{F}(\boldsymbol{x},\tilde{\boldsymbol{b}}) + \boldsymbol{\epsilon}, \tag{2}$$

where $\tilde{\boldsymbol{b}}$ are parameters not being retrieved but which influence the forward model results. The forward model approximates the true physical relation between $\boldsymbol{x}$ and $\boldsymbol{y}$, and there are uncertainties associated with both the observations $\boldsymbol{y}$ and the forward model parameters $\tilde{\boldsymbol{b}}$. $\boldsymbol{\epsilon}$ represents the total uncertainty due to all sources. OE attempts to find $\hat{\boldsymbol{x}}$, an estimate of the state which maximizes the posterior conditional probability density function (PDF) $P(\boldsymbol{x} \mid \boldsymbol{y})$, subject also to prior knowledge about the values of $\boldsymbol{x}$. This prior knowledge is described by expected values $\boldsymbol{x}_a$ and their covariances $\mathbf{S}_a$. Assuming Gaussian statistics for the model-measurement errors and the a priori state, minimizing the cost function

$$\Phi(\boldsymbol{x},\boldsymbol{y},\boldsymbol{x}_a) = \left(\boldsymbol{y} - \boldsymbol{F}(\boldsymbol{x},\tilde{\boldsymbol{b}})\right)^{\mathsf{T}} \mathbf{S}_{\epsilon}^{-1} \left(\boldsymbol{y} - \boldsymbol{F}(\boldsymbol{x},\tilde{\boldsymbol{b}})\right) + (\boldsymbol{x} - \boldsymbol{x}_a)^{\mathsf{T}} \mathbf{S}_a^{-1} (\boldsymbol{x} - \boldsymbol{x}_a), \tag{3}$$

with respect to $\boldsymbol{x}$ gives this PDF, where $\mathbf{S}_\epsilon$ is the covariance matrix representing the uncertainties $\boldsymbol{\epsilon}$. The Gaussian assumption is reasonable if the expected values and covariance matrices are known for the model-measurement uncertainties and the a priori state, but other details are lacking. In that case, the Gaussian form maximizes the entropy of a PDF (Shannon and Weaver, 1949; Rodgers, 2000). Assuming an alternate form would introduce constraints on the retrieval that are not justified based on the limited knowledge of the PDF.

Provided the forward model is not excessively nonlinear, Newtonian iteration

$$\hat{\boldsymbol{x}}_{i+1} = \hat{\boldsymbol{x}}_i + \left(\mathbf{S}_a^{-1} + \mathbf{K}_i^\mathsf{T}\mathbf{S}_\epsilon^{-1}\mathbf{K}_i\right)^{-1}\left[\mathbf{K}_i^\mathsf{T}\mathbf{S}_\epsilon^{-1}\left(\boldsymbol{y} - \boldsymbol{F}(\hat{\boldsymbol{x}}_i, \tilde{\boldsymbol{b}})\right) - \mathbf{S}_a^{-1}(\hat{\boldsymbol{x}}_i - \boldsymbol{x}_a)\right], \tag{4}$$

leads to $\hat{\boldsymbol{x}}$, where $\mathbf{K}$ is the Jacobian of the forward model with respect to $\boldsymbol{x}$, and $\mathbf{K}_i = \mathbf{K}(\hat{\boldsymbol{x}}_i)$. Iteration continues until the ~~covariance-weighted~~ squared difference in successive $\hat{\boldsymbol{x}}_i$ normalized by the current estimate of the a posteriori covariance $\hat{\mathbf{S}}_x$ is much smaller than the number of state vector elements (Rodgers, 2000). At convergence, ~~the~~ this covariance of $\hat{\boldsymbol{x}}$ is obtained as

$$\hat{\mathbf{S}}_x = \left(\hat{\mathbf{K}}^\mathsf{T}\mathbf{S}_\epsilon^{-1}\hat{\mathbf{K}} + \mathbf{S}_a^{-1}\right)^{-1}, \tag{5}$$

where $\hat{\mathbf{K}} = \mathbf{K}(\hat{\boldsymbol{x}})$. As a diagnostic test of the results, a χ^2 statistic is calculated using the retrieved state vector in Eq. (3). A value near the number of observations suggests correct convergence (Marks and Rodgers, 1993). Several metrics, determined from the retrieved state and based in information theory, provide insight into the retrieval performance; these metrics are presented in Sect. 4.

2.1 The forward model

To assess the information provided purely by reflectivity observations, whether from ground-, aircraft-, or space-based radars, the retrieval ignores attenuation and multiple scattering. This treatment would be appropriate for cases with little intervening scattering and extinction between the radar and observed snowfall, such as when the radar bin containing the snowfall of interest is near the radar or under light snowfall conditions. For such a case, the singly-scattered reflectivity Z_e^{ss} as a function of range R from the radar is given by

$$Z_e^{ss}(R) = \frac{\Lambda^4}{\|K_w\|^2\pi^5}\int_{D_{min}}^{D_{max}} N(D,R)\sigma_{bk}(D,R)dD \tag{6}$$

where $\sigma_{bk}(D,R)$ is the backscatter cross-section for particle size D at range R, $N(D,R)$ is the particle size distribution (PSD) at range R, Λ is the radar wavelength, and K_w is the dielectric factor for water.

2.1.1 Forward model parameters: snow particle model

Backscattering and extinction cross-sections depend intimately on particle mass, shape and orientation relative to the radar beam. These properties are highly variable for snow particles, and the approach used here is to specify their PDFs a priori using best estimates and treat their variability as a source of uncertainty in the retrieval. We adopt the common model (e.g., Locatelli and Hobbs, 1974; Mitchell, 1996) in which mass and horizontally-projected area are described using power laws

$$m(D_M) = \alpha D_M^\beta \tag{7}$$

$$A_p\left(D_M\right) = \gamma D_M^{\sigma} \tag{8}$$

on particle maximum dimension, D_M, and use the particle properties and shape "B8pr-30" (Wood et al., 2015), an idealized branched spatial particle that was found to minimize bias in simulated reflectivies versus coincident W-band radar observations. That work used in-situ ~~and remote sensing~~ measurements and remotely-sensed X-band reflectivity observations of snow from C3VP (Hudak et al., 2006) along with previously reported single-particle measurements to develop best estimates and covariances for the power law parameters α, β, γ, and σ. These results then constrained discrete dipole approximation calculations using DDSCAT (Draine and Flatau, 1994) to obtain best estimates of snow particle single-scattering properties and their uncertainties at the desired wavelengths. These a priori descriptions of size-resolved particle mass, A_p, σ_{bk}, σ_{ext} and their uncertainties constitute the particle model used in the retrieval and are summarized in Appendix B.

2.2 The retrieved state

The relationship described by Eq. (6) requires information about particle size distributions and single-scattering properties. With scattering properties and their uncertainties specified a priori as described in section 2.1.1, this leaves the snow PSD parameters and their PDFs to be determined by the retrieval.

Snow PSDs are frequently characterized as exponential

$$N(D) = N_0 \exp\left(-\lambda D\right) \tag{9}$$

where λ is the slope of the distribution and N_0 its intercept. Rogers (1973) used photographs of snowflakes to develop estimates of snow size distributions based on actual dimensions and found snow size distributions to be exponential. Brandes et al. (2007) evaluated both exponential and gamma forms, which have the ability to represent sub- or super-exponential behavior, for snow size distributions observed by a 2D video disdrometer over the course of several winter seasons. Although about 22% of the observed snow distributions exhibited super-exponential features, more commonly the fitted gamma distributions were nearly equivalent to exponential distributions. Several aircraft-based studies using in situ observations under a wide range of atmospheric conditions have confirmed exponential behavior, especially at larger particle sizes (Passarelli, 1978; Houze et al., 1979; Lo and Passarelli, 1982; Gordon and Marwitz, 1984; Braham, 1990; Woods et al., 2008) . While other studies of aircraft observations have noted departures from exponential behavior (e.g., "super-" or "sub-exponential", Herzegh and Hobbs, 1985), Heymsfield et al. (2008) examined the suitability of exponential distributions for snow. They found that fitted exponential distributions, when used to simulate IWC and Ze, could provide generally good agreement with IWC and Ze calculated directly from the observed discrete size distributions. These studies support the adequacy of exponential distributions for retrieving snowfall. D may be an actual dimension of the snow particle, the diameter of an equivalent mass ice sphere, or the melted drop diameter. The choice is significant because N_0 and λ depend on the choice of D. For this work, we use the maximum particle dimension, D_M, because D_M is closely related to the particle dimensions measured by imagers such as video disdrometers (Wood et al., 2013) and aircraft particle probes, making comparisons with other datasets more straightforward.

The exponential size distribution parameters N_0 and λ are the desired state variables. Values for N_0 may range over several orders of magnitude, so $\log(N_0)$ is retrieved instead. The variability of λ is significantly smaller than that of N_0; however, examination of fitted exponential distributions from C3VP snow events indicated that the distribution of values for λ was strongly non-Gaussian. The log-transformed values are much less skewed (Fig. 1a), and accordingly, log(λ) is retrieved instead . The corresponding state vector to be retrieved is then

$$\hat{\boldsymbol{x}} = \begin{bmatrix} \log(N_0) \\ \log(\lambda) \end{bmatrix}, \tag{10}$$

and the associated covariance matrix obtained from the retrieval is of the form

$$\hat{\mathbf{S}}_x = \begin{bmatrix} s^2(\log(N_0)) & s(\log(N_0), \log(\lambda)) \\ s(\log(N_0), \log(\lambda)) & s^2(\log(\lambda)) \end{bmatrix}. \tag{11}$$

2.3 Prior estimates of the state

For each profile, the a priori state consists of a vector of expected values $\boldsymbol{x}_a$ and the corresponding covariance matrix $\mathbf{S}_a$, having the same sizes as the state vector $\boldsymbol{x}$ (Eq. (10)) and its covariance matrix $\mathbf{S}_x$ (Eq. (11)). A priori estimates of $\log(N_0)$ and $\log(\lambda)$ are determined using temperature-based parameterizations derived using snow PSDs observed during C3VP and other field experiments. Exponential size distributions were fit to the observed size spectra from both ground-based Snowflake Video Imager, or SVI (Newman et al., 2009; Wood et al., 2013), and from 2D particle probes carried aboard the National Research Council Canada's Convair-580 during three C3VP research flights (Fig. 1b). Results from a number of earlier studies are shown as well for comparison, including ground-based observations taken in and near the Rocky Mountain Front Range (Rogers, 1973; Brandes et al., 2007); and aircraft observations over the central Sierra Nevada (Gordon and Marwitz, 1984, 1986), in lake effect snow over Lake Michigan (Braham, 1990), in synoptic snowfall over central Illinois (Passarelli, 1978), and in orographic and frontal wintertime precipitation in the Pacific ~~Northwest~~ Northwest (Woods et al., 2008). Also shown are similar fits performed on 2D probe observations from a Wakasa Bay research flight on 27 January 2003 (Lobl et al., 2007). The results suggest that the C3VP observations adequately represent snowfall from a number of different regimes, although the number concentrations from several studies are at the margins of the C3VP observations.

Both λ and N_0 have been observed to vary log-linearly with temperature (e.g., Houze et al., 1979; Woods et al., 2008; and works reviewed in Ryan, 1996). Fits were therefore constructed for both parameters using the combined C3VP aircraft and SVI data and uncertainties estimated using residual standard deviations (RSDs) calculated for data binned into 2 K intervals (Fig. 2). The narrow temperature ranges for the Wakasa Bay and Brandes et al. (2007) observations make comparisons against the C3VP temperature dependence uninformative. For λ, the Rogers (1973) observations are largely outside the bounds of the RSDs, but are generally consistent with the C3VP histogram for warmer temperatures. The aircraft observations other than Wakasa Bay follow a temperature trend similar to the C3VP observations. For N_0, several of the comparison datasets lie mostly above the RSD bounds, but would be well within a +2 RSD bound.

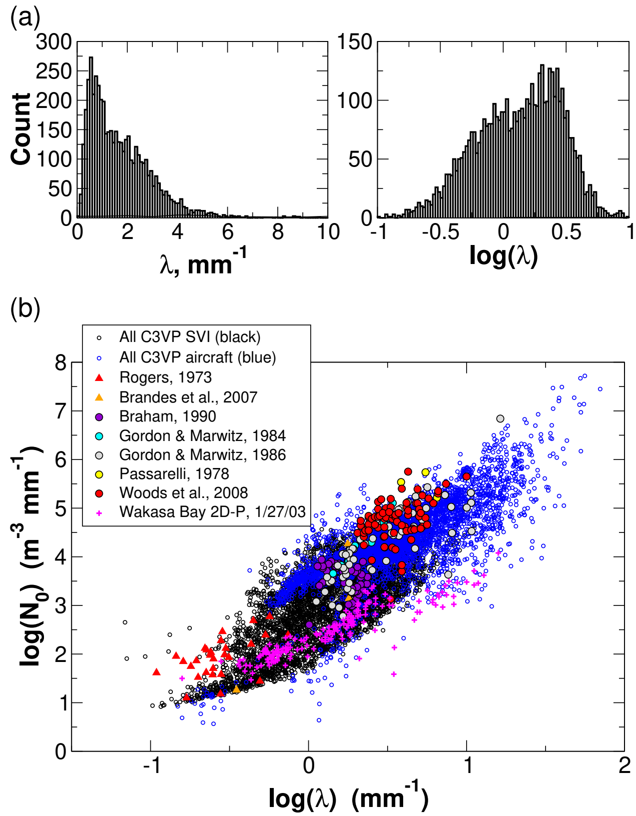

Figure 1. a) Histograms of λ and $\log(\lambda)$ fitted to C3VP SVI observations. b) Estimates of λ and N_0 determined from fits to size distributions from C3VP observations, with values provided from several earlier studies for comparison.

Based on the similarity of C3VP with results from other experiments, the a priori states derived from these observations can be expected to represent a broad range of snowfall regimes and were adopted for the retrieval. A priori values for $\log(\lambda)$ and $\log(N_0)$ were estimated from the linear fits as

$$\begin{aligned} \log(\lambda_{ap}) &= -0.03053(T-273.)-0.08258 \\ \log(N_{0,ap}) &= -0.07193(T-273.)+2.665 \end{aligned} \tag{12}$$

with λ in mm^{-1}, N_0 in $\mathrm{m}^{-3}\ \mathrm{mm}^{-1}$, and T in K. The RSDs show little variation with temperature except in the vicinity of 240 K, where they increase substantially. These large RSDs are in response to a few outlying samples with small λ and N_0 values. Accordingly, variances were treated as constant and were estimated as the squared RSDs averaged over all temperatures. The uncertainty model also includes the covariance between $\log(N_0)$ and $\log(\lambda)$. Correlation coefficients were evaluated for each of the temperature-binned data subsets. giving a mean coefficient of 0.72 with a standard deviation of 0.12. The a priori covariance was modeled as $0.72 \cdot s(\log(\lambda_{ap})) \cdot s(\log(N_{0,ap}))$:

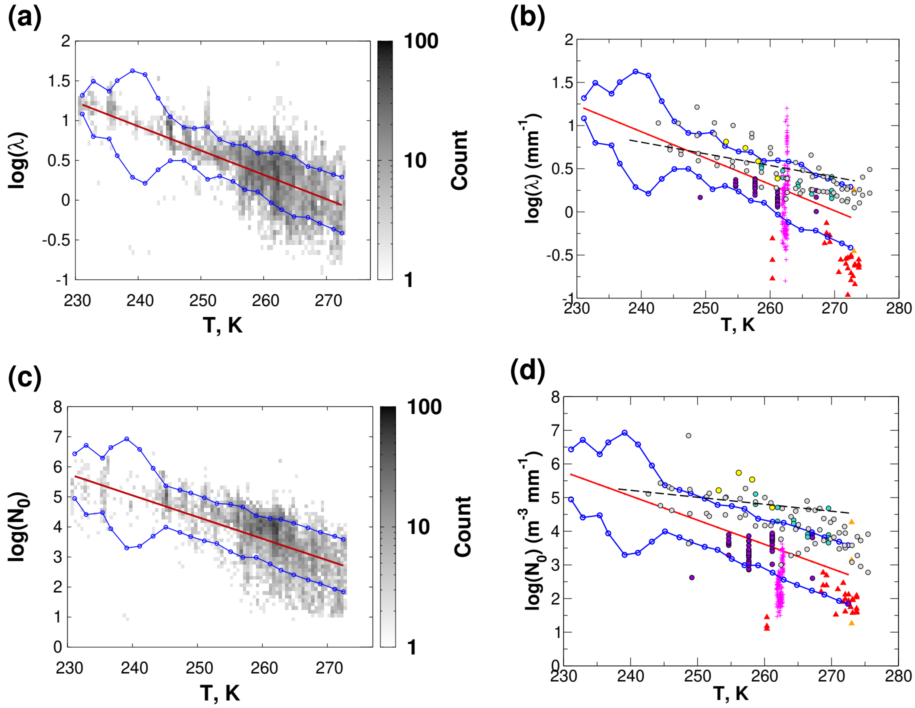

Figure 2. Dependence of $\log(\lambda)$ and $\log(N_0)$ on temperature. Central red lines show the best-fit relationships, while the upper and lower blue lines show bounds given by +/- 1 residual standard deviation. The shaded gray shows the 2D histogram of values for the C3VP surface and aircraft observations (panels a and c). Symbols (panels b and d) match those from Figure 1 except that, in lieu of symbols for Woods et al. (2008), the dashed black line shows a linear best fit reported by the authors.

$$\begin{aligned} s^2\left(\log\left(\lambda_{ap}\right)\right) &= 0.133 \\ s^2\left(\log\left(N_{0,ap}\right)\right) &= 0.95 \\ s\left(\log\left(\lambda_{ap}\right), \log\left(N_{0,ap}\right)\right) &= 0.26 \end{aligned} \tag{13}$$

3 Implementation and uncertainty sources

Applying the exponential distribution in Eq. (6), the singly-scattered nonattenuated reflectivity Z_e^{ss} is

$$Z_e^{ss}(R) = \frac{\Lambda^4}{\left\|K_w\right\|^2 \pi^5} \int\limits_{D_{M,min}}^{D_{M,max}} N_0 \exp\left(-\lambda D_M\right) \sigma_{bk}(D_M, \tilde{\boldsymbol{b}})\, dD_M. \tag{14}$$

The backscatter cross-section σ_{bk} has been written to show its dependence on a vector of parameters $\tilde{\boldsymbol{b}}$ as well as on D_M. The vector $\tilde{\boldsymbol{b}}$ includes the parameters for the mass- and area-dimension relations α, β, γ, and σ which were used to construct the particle models from which the scattering properties were calculated. The tilde indicates that these parameters are approximations of the true values and a source of uncertainty.

3.1 Model-measurement uncertainties

The error covariance matrix $\mathbf{S}_\epsilon$ is

$$\begin{aligned}\mathbf{S}_\epsilon &= \mathbf{S}_y + \mathbf{S}_F \\ &= \mathbf{S}_y + \mathbf{S}_B^{ss} + \mathbf{S}_F^{ss}\end{aligned} \tag{15}$$

where $\mathbf{S}_y$ is the covariance matrix for the measurement uncertainties and ~~$\mathbf{S}F$~~ $\mathbf{S}_F$ is that for the singly-scattered reflectivities given in Eq. (14). The forward-model uncertainties may be further decomposed as the sum of two terms: $\mathbf{S}_B^{ss}$, which is a covariance matrix describing uncertainties due to the forward model parameters $\tilde{\boldsymbol{b}}$, and $\mathbf{S}_F^{ss}$, which is a covariance matrix describing uncertainties due to other assumptions in the calculation of Z_e^{ss}.

3.1.1 Uncertainties for measured reflectivities

The sources of reflectivity measurement ~~uncertainty $\mathbf{S}_y$ include uncertainty~~ error include errors in the absolute radiometric calibration and measurement noise. For this work, we assume the radar is well-calibrated, leaving noise as the uncertainty source~~, and model~~. To estimate $\mathbf{S}_y$, we model the noise using the well-characterized CloudSat CPR (Tanelli et al., 2008). For reflectivities above -10 dBZ, one standard deviation of noise as a fraction of the mean signal is about -16 dB, while for reflectivities below -10 dBZ, noise is an increasing fraction of the signal, reaching 0 dB at the minimum detectable signal of -30 dBZ (R. Austin, personal communication, 4 November, 2008). The resulting uncertainties range from 3 dBZ for a reflectivity of -30 dBZ to about 0.1 dBZ for reflectivities above -10 dBZ$_e$. (Fig. 3).

3.1.2 Forward model uncertainties

Uncertainties $\mathbf{S}_B^{ss}$ due to the forward model parameters $\tilde{\boldsymbol{b}} = (\alpha, \beta, \gamma, \sigma)^\mathsf{T}$ that describe the snow particle model were examined in Wood et al. (2015) as

$$\mathbf{S}_B^{ss} = \mathbf{K}_b \mathbf{S}_b \mathbf{K}_b^\mathsf{T} \tag{16}$$

where $\mathbf{K}_b$ is the Jacobian of the forward model reflectivities with respect to the parameters $\tilde{\boldsymbol{b}}$ and $\mathbf{S}_b$ is the covariance matrix for the parameters. The Jacobian $\mathbf{K}_b$ depends on the estimated state $\hat{\boldsymbol{x}}$ and ~~so is evaluated~~ is computed at each iterative step~~via finite differences using a set of perturbed particle models~~. At each step, the forward model is used to calculate reflectivity perturbations that result from perturbations of the parameters α, β, γ, and σ. The ratio of each reflectivity perturbation to its parameter perturbation gives an element of the Jacobian. The parameter perturbation affects the reflectivity via changes to the corresponding particle scattering properties. The perturbed scattering properties are precomputed with

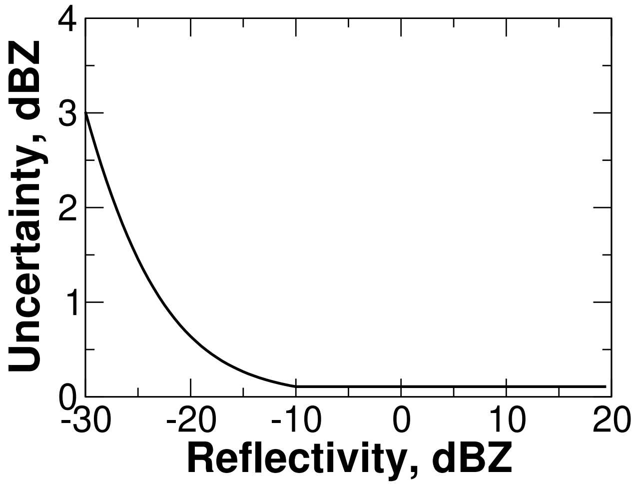

Figure 3. ~~Uncertainty~~ Estimated measurement uncertainty, based on one standard deviation of noise for the CloudSat CPR.

DDSCAT (Draine and Flatau, 1994) by using the perturbed parameter to generate discrete dipoles models following the process described in Wood et al. (2015). Wood et al. (2015) found ~~these~~ the resulting forward model uncertainties to be near 5 dB, increasing to as high as 15 dB for very broad distributions.

$\mathbf{S}_F^{ss}$ quantifies uncertainties due to other assumptions and limitations in the forward model reflectivity calculation. Wood et al. (2015) looked at uncertainties due to the random component of dipole placement within DDA models for a particular particle shape and found them negligible. Other sources include the assumption of the shape of the distribution as exponential, the choice of particle shape, and the discretization and truncation of the integrations over size distribution.

Errors due to the assumed exponential shape were evaluated using a dataset of 4080 SVI-measured, discrete, 5-minute-duration snow PSDs from C3VP. Simulated reflectivities and snowfall rates were calculated using the B8pr-30 particle model and the Mitchell and Heymsfield (2005) terminal velocity model. Exponential distributions were fit to the observed discrete PSDs using orthogonal distance regression (Boggs et al., 1992; Jones et al., 2001) with uncertainty estimates per Wood et al. (2013). The fitted distributions were scaled in number concentration to match the snowfall rates simulated from the discrete distributions. The fitted distributions were then used to simulate reflectivities for comparison against those from the discrete distributions. Errors are negligible at high reflectivities but increase as reflectivity decreases (Fig. 4). Bias is negligible, and the total uncertainty is modeled as

$$s_F^2\,(dB) = \left[\exp\left(-\left(dBZe+14\right)/16\right)\right]^2, \tag{17}$$

reaching a maximum of 1 dB of uncertainty at -15 dBZe.

Uncertainties due to shape were evaluated using the same SVI dataset to which the alternate particle shapes Ep (ellipsoidal) and B8pr-45 (branched spatial particle with larger aspect ratio than B8pr-30) from Wood et al. (2015) were applied to simulate reflectivities. These alternate shapes are constrained to have the same mass-dimension relationship as used for the B8pr-30

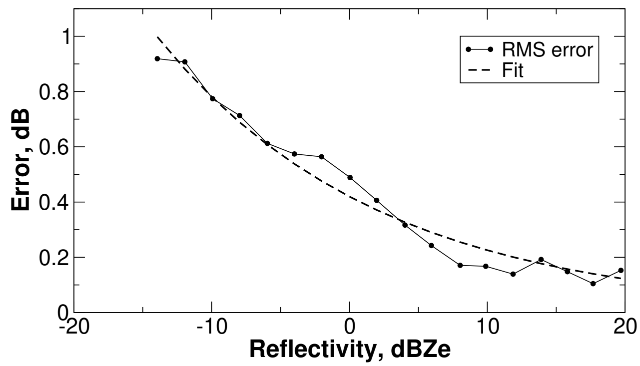

Figure 4. Actual RMS errors and the fitted model for uncertainty due to the assumed exponential size distribution.

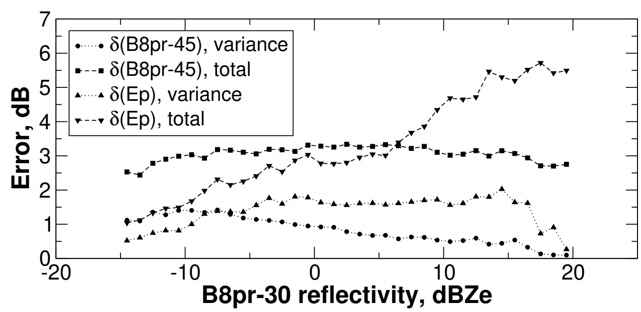

Figure 5. Errors in reflectivity for the Ep and B8pr-45 shapes compared to the B8pr-30 shape. Errors shown are total (bias + variance) and variance only.

particle model used in this work, so differences are due only to particle shape. Figure 5 shows total and variance-only RMS errors. From these results we estimate the shape uncertainty to be 2 dB.

Finally, truncation and discretization errors were evaluated using the same SVI PSD dataset. These are errors that result from the discrete treatment of the integrations over size distribution, errors due to both the limited maximum D_M in the particle model and in the limited resolution of the particle model. Truncation errors were evaluated using analytic exponential PSDs fitted to the SVI PSD dataset as described previously. The particle model backscatter properties were augmented to $D_M = 40\,\mathrm{mm}$ by linearly extrapolating backscatter efficiencies, then reflectivities were calculated using integrations to both the standard (maximum $D_M = 18\,\mathrm{mm}$) and augmented size range. The bias and scatter of the truncation errors were -0.1 and 0.42 dB. To evaluate discretization errors, a high-resolution version of the particle model backscatter properties was created by interpolating backscatter efficiencies so that the particle size resolution of the particle model was increased by a factor of two. Reflectivities were then calculated and compared against those from the standard-resolution particle model. The bias and scatter of the discretization errors were ~~0.~~ 0.00 and 0.02 dB.

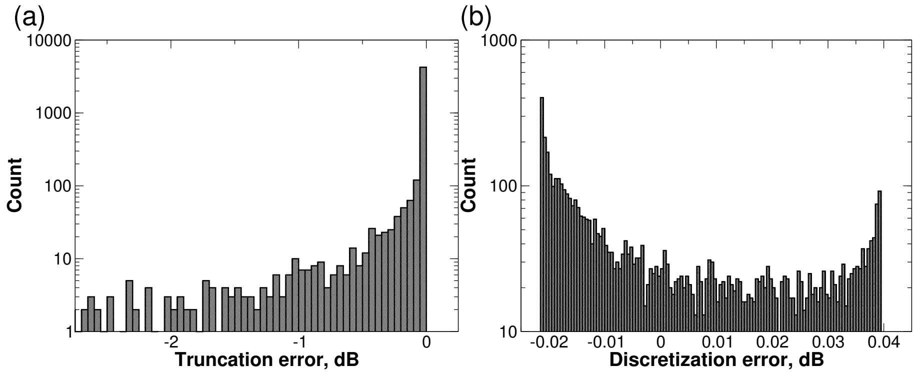

Figure 6. Histograms of errors for truncation and discretization.

3.2 Snowfall rate and uncertainties

The snowfall rate P in units of liquid water depth per unit time is

$$P(R) = \frac{1}{\rho_{liq}} \int\limits_{D_{M,min}}^{D_{M,max}} N(D_M,R)m(D_M,R)V(D_M,R)\,dD_M, \tag{18}$$

where $m(D_M,R)$ is particle mass, $V(D_M,R)$ is fallspeed, and ρ_{liq} is the density of liquid water. Particle mass is provided by Eq. (7). Fallspeed is assumed to equal terminal velocity, which is calculated from the model of Mitchell and Heymsfield (2005) using particle mass, the horizontally-projected area from Eq. (8), and environmental pressure and temperature from collocated observations. Uncertainties for the estimated snowfall rate are determined in a manner similar to that used for the forward model uncertainties. The total variance $\mathbf{S}_P$ is decomposed as

$$\mathbf{S}_{pP} = \mathbf{S}_{\hat{x}\hat{x},P} + \mathbf{S}_{\tilde{b}\tilde{b},P} + \mathbf{S}_{vv,P} + \mathbf{S}_{expexp,P} \tag{19}$$

where the terms on the right represent the variances resulting from 1) retrieved state uncertainties, 2) particle model parameter uncertainties, 3) uncertainties in the fallspeed model and its parameters, and 4) assuming an exponential form for the PSD, respectively.

Contributions from uncertainties in the retrieved state and in the particle model parameters are determined using linearized error propagation (e.g., following a form like Eq. (16)). For $\mathbf{S}_{\tilde{b},P}$, which gives the snowfall rate variance that results from uncertainties in the particle model parameters, this means that the Jacobian $\mathbf{K}_{\tilde{b},P}$ is calculated for the snowfall rate with respect to the particle model parameters α, β, γ, and σ, following the process described for the reflectivity Jacobian in section 3.1.2. Then

$$\mathbf{S}_{\tilde{b},P} = \mathbf{K}_{\tilde{b},P}\mathbf{S}_b\mathbf{K}_{\tilde{b},P}^{\mathsf{T}} \tag{20}$$

where $\mathbf{S}_b$ is the covariance matrix for the particle model parameters as determined in Wood et al. (2015).

Fallspeed contributions are handled following Wood et al. (2014). Snowfall rate uncertainties due to the assumed exponential form of the size distribution are determined using the SVI PSD dataset in an approach analogous to that for Eq. (17). In this approach, number concentrations for the fitted exponential distributions were scaled so that reflectivities were matched, then snowfall rate errors were evaluated. The fractional uncertainty in snowfall rate was found to be

$$f_P = -0.06\log(P) + 0.05 \tag{21}$$

from which the necessary variance can be determined. Uncertainties from each of the four sources are treated as uncorrelated.

4 Retrieval performance tests with ground-based radar observations

During C3VP, a vertically-pointing W-band radar (the Jet Propulsion Laboratory's Airborne Cloud Radar, ACR) was deployed on the ground at CARE. In all, about 28 hours of ACR radar profiles of snowfall were recorded at approximately 2.8 s intervals. These observations represent 17 distinct snow events that occurred over 18 days between 3 November 2006 and 2 March 2007; however, most of the accumulations were concentrated during nine of the events (Table 1). ~~The data include~~ These observations include portions of three of the cases that were used to develop the snow particle microphysical ~~and scattering models (Wood et al., 2015)~~models (cases SYN1, LES1, and LES2, (Wood et al., 2015)). Of the nearly 36,000 ACR profiles in these observations, approximately 7300 are from ~~these three cases .~~ cases SYN1, LES1 and LES2. Further, as described in Wood et al. (2015), ACR reflectivities from 12 of the events between 2 December 2006 and 26 Febraury 2007 were used to constrain the snow particle models' scattering properties to give unbiased reflectivities. This overlap should be kept in mind when evaluating the retrieved snowfall rates and estimated accumulation, but it should not substantially affect the assessements of retrieval uncertainties, uncertainty sources, and information content metrics that follow.

The retrieval was applied to the ACR reflectivities observed in the single range bin nearest the surface, at 197 m above ground level (AGL). Temperatures and pressures needed by the retrieval to perform snow detection, calculate fallspeeds and establish the a priori states were obtained from nearby surface meteorology observations. Because of the short distance to the target range bin, attenuation along the path was neglected. The retrieved snowfall rates produce a Z-S relationship that is most similar to that developed by Kulie and Bennartz (2009) for an aggregate particle model denoted as HA (Fig. 7). For warmer temperatures and mid-range reflectivites, the Z-S relationship becomes more similar to that of Liu (2008) and the LR3 relationship of Kulie and Bennartz.

For comparisons, snowfall rate observations were obtained at 1-minute intervals from the Vaisala FD12P (Vaisala Oyj, 2002) and scaled to provide unbiased accumulations relative to the nearby Dual Fence Intercomparison Reference, or DFIR (Goodison et al., 1998). The retrieved ACR snowfall rates, P_{ACR}, were matched to the nearest-in-time observed snowfall rate, P_{FD12P}.

Time series of P_{ACR} and P_{FD12P} show a high degree of agreement over most of the observing period (Fig. 8, upper panel). This is not extraordinary given the dependence of the retrieval's particle microphysical and scattering properties on portions of the C3VP data. Two notable exceptions occur near time indices 25000 and 32500, however, when the FD12P recorded

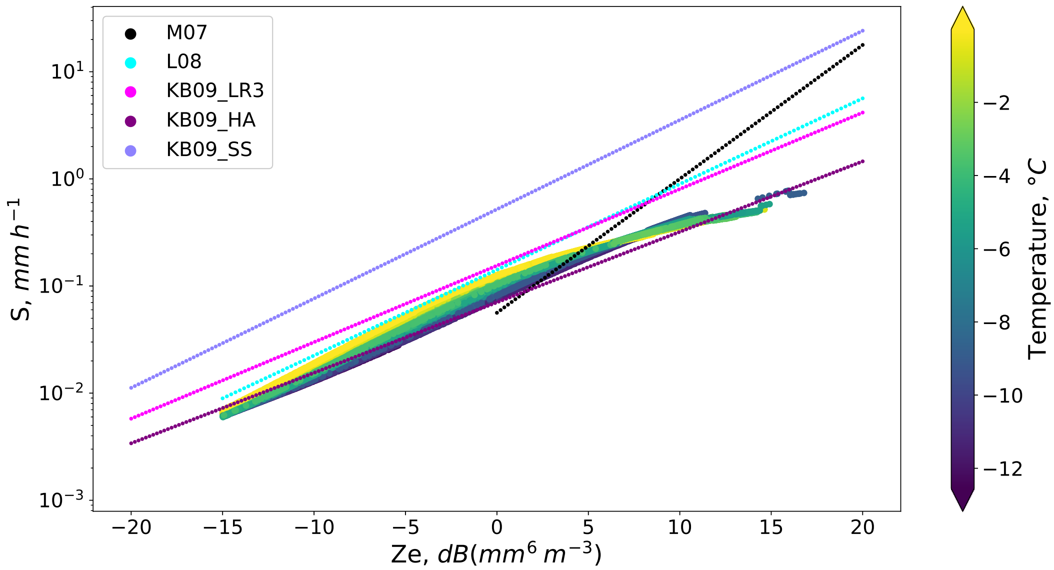

Figure 7. Z-S values as a function of temperature for this retrieval compared against those from: M07, Matrosov (2007); L08, Liu (2008); and KB09_LR3, KB09_HA, and KB09_SS, Kulie and Bennartz (2009).

snowfall rates above 1 mm LWE h^{-1} while the retrieved values are substantially smaller. Examining the time series of ACR reflectivities shows that the ACR did not observe high reflectivities during these periods (Fig. 8, lower panel). The first of these anomalies occurred 22 February 2007 from 11:20 to 12:05 UTC while the second occurred 1 March 2007 between 22:15 and 22:50 UTC. For both, the ACR operator made note of the heavy snowfall, suggesting that both the FD12P and the ACR observed similar snowfall rates (Austin et al., 2007). Based on soundings, Environment Canada forecasts, and ACR operator observations, these anomalies appear to correspond with melting aloft, ice pellets, and freezing rain (Wood, 2011). These conditions could also have been favorable for formation of large, heavy aggregates. It seems likely that the conditions produced snowfall whose properties were strongly inconsistent with the particle properties assumed in the retrieval, ~~which violate the retrieval's assumption of dry, aggregate-like snow particles~~although reflectivities did not change substantially.

Accumulations were calculated from both P_{ACR} and P_{FD12P} with and without the two anomalies described above (Fig. 9). Accumulations agree substantially during the first 16 hours but diverge somewhat beyond that, again noting the dependence of the retrieval's assumed microphysical and scattering properties on portions of the C3VP data. With the anomalies included the final difference between the accumulations is 2 mm. With the anomalies removed that difference is reduced to 0.7 mm. For individual events, absolute fractional differences between the ACR and FD12P accumulations can range to 50% and upwards (Table 1), but these large values are associated mainly with events with small accumulations. For events with larger accumulations, the absolute fractional differences are mostly below 30%. At seasonal timescales, the random components in event-total accumulations are likely uncorrelated, leading to offsetting errors when calculating seasonal accumulations. The time series of absolute fractional differences between the ACR-derived and FD12P accumulations begins with large fractional

Table 1. Accumulations by event for the ACR retrievals. Two distinct events, indicated as (a) and (b), occurred on 20 Jan 2007. Duration shows the elapsed time of ACR observations for which retrievals were performed. Fractional differences are relative to FD12P accumulations. *Accumulations adjusted to remove anomalies indicated in Figure 8.

		Accumulations		
Date	Duration	ACR	FD12P	Fractional
	h	mm LWE		difference, %
3 Nov 2006	0.98	0.065	0.11	-40.9%
2 Dec 2006	0.16	0.007	0.00	—
6 Dec 2006	4.00	0.86	0.80	7.5%
7 Dec 2006	1.08	0.038	0.093	-59.1%
8 Dec 2006	0.34	0.018	0.00	—
17 Jan 2007	0.09	9.3e-04	0.00	—
19 Jan 2007	0.46	0.061	0.13	-53.1%
20 Jan 2007 (a)	0.32	0.004	2.8e-04	1329%
20 Jan 2007 (b)	0.59	0.079	0.0	—
22 Jan 2007	4.29	0.89	0.87	2.2%
23 Jan 2007	0.76	0.017	0.00	—
26 Jan 2007	0.93	0.045	0.085	-47.1%
27 Jan 2007	3.36	0.57	1.06	-46.2%
19 Feb 2007	0.97	0.26	0.18	44.4%
22 Feb 2007	2.72	0.40*	0.23*	73.9%
26 Feb 2007	2.41	0.58	0.64	9.4%
1 Mar 2007	4.23	1.14*	1.57*	-27.4%
Season	26.3	5.04*	5.77*	-12.6%

differences. Within 5 hours and over the initial three events, the fractional differences reduce to less than 5%, then remain below 20% for the remainder of the season.

4.1 Snowfall rate uncertainties

Uncertainties in instantaneous snowfall rate estimates, taken to be the square root of the total variance evaluated as shown in Eq. (19), were evaluated by binning the fractional uncertainties by snowfall rate then averaging and taking standard deviations. Mean fractional uncertainties range from 150% to 185%, and the range for +/- 1 standard deviation extends from about 145% to 190% (Fig. 10). The fractional uncertainties generally increase with increasing snowfall rate, but above 0.5 mm LWE h^{-1} the means and standard deviations diminish and result from only a small number of samples in each bin. For comparison, uncertainties for FD12P precipitation rates at 5-minute resolution were estimated at 0.03 mm h^{-1} for rates less than 0.05 mm

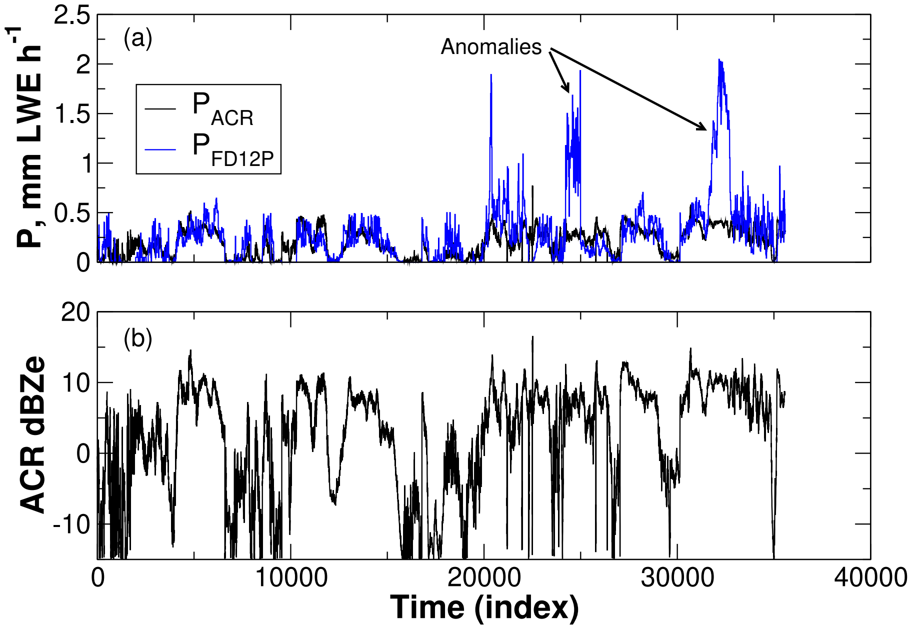

Figure 8. Upper panel: Time series of snowfall rates retrieved from ACR reflectivities and observed. Lower panel: Corresponding time series of ACR reflectivities. Each time index indicates a 2.8 s observation by the ACR. Snowfall rates retrieved for the ACR used the reflectivity in the range bin nearest the surface, at 197 m AGL.

h^{-1}, 50% for rates up to 0.5 mm ~~unith~~h^{-1}, and 30% for rates larger than 0.5 $\mathrm{mm\ h}^{-1}$ by Wood et al. (2014) based on comparisons against a Precipitatation Occurrence Sensor System.

To evaluate the importance of each source of uncertainty, variances from each of the sources from Eq. (19); (retrieved state, microphysical parameters, fallspeed parameterization, or exponential distribution) were extracted separately, then fractions of total variance were calculated. To allow the trends in each source to be shown as a function of snowfall rate (Fig. 11), the fractions were binned by snowfall rate and averaged. As snowfall rates increase up to 0.5 $\mathrm{mm\ h}^{-1}$, the variance due to the retrieved state becomes a more significant contributor to the total variance, while the contributions from the other sources diminish. The contribution due to the assumed exponential PSD shape is not significant.

The instantaneous uncertainties for snowfall rate include uncertainties due to random errors and biases in the retrieval components and observations. For accumulations or mean rates evaluated over longer time periods, errors due to random sources may be reduced and remaining errors can be more representative of biases in the retrieval. The reductions in random errors depend on their correlations in time, however (e.g., Taylor, 1997). When random errors within events are assumed perfectly positively correlated, end-of-event P_{ACR} accumulations have fractional uncertainties from 1.5% to 52.4% (Fig. 12). In actuality, the random error sources likely decorrelate with increasing separation in time. While the scales for these decorrelations are not known, with even a modest amount of decorrelation in the errors the uncertainties are reduced substantially. After applying a negative exponential decorrelation model with a decorrelation scale of 0.5 hour to intra-event errors, the fractional uncertain-

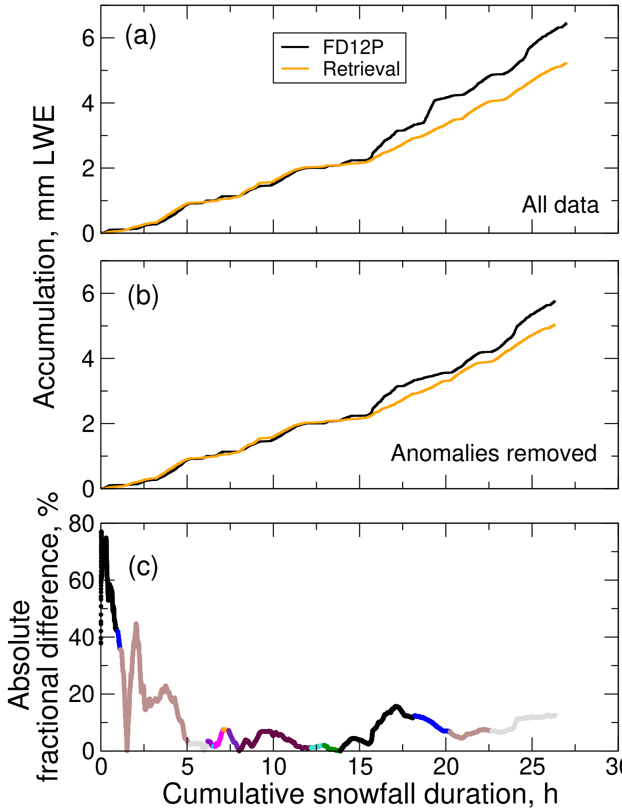

Figure 9. Snow accumulations computed from P_{ACR} and P_{FD12P}. The accumulations are for 17 snow events observed by the ACR on 18 days between 3 November 2006 and 2 March 2007, but accumulations are principally from nine events (Table 1). The events were concatenated sequentially in time and the time axis indicates the cumulative time over all events. (a) Accumulations from all observations and corresponding retrieval results, (b) accumulations with two anomalous periods identified in Figure 8 removed, and (c) fractional differences in accumulations shown in panel (b), with distinct colors indicating individual events.

ties at the ends of individual events are 1.3% to 18.8%. The most significant reductions due to decorrelation occur with the longer-duration events. The end-of-season P_{ACR} accumulation uncertainties, calculated assuming inter-event uncertainties are uncorrelated, are reduced from 64.9% for perfectly correlated to 11.8% for decorrelated intra-event errors.

Agreement between observed P_{FD12P} event accumulations and those from P_{ACR} generally improves for events with larger accumulations and durations (Fig.12). Of the seven events with accumulations larger than 0.2 mm and durations of 1 h and longer, the P_{FD12P} accumulations for six fall within or near the uncertainty bounds of the P_{ACR} accumulations with perfectly correlated errors, while four out of seven are within or near the much narrower bounds for errors with decorrelations. This result is also true for the season as a whole. For the duration of 26.3 hours and accumulation of 5.05 mm from P_{ACR}, the difference compared to the P_{FD12P} seasonal accumulation of 5.77 mm is -12.6%. The difference is similar to the P_{ACR} accumulation uncertainty of 11.7% for decorrelated errors.

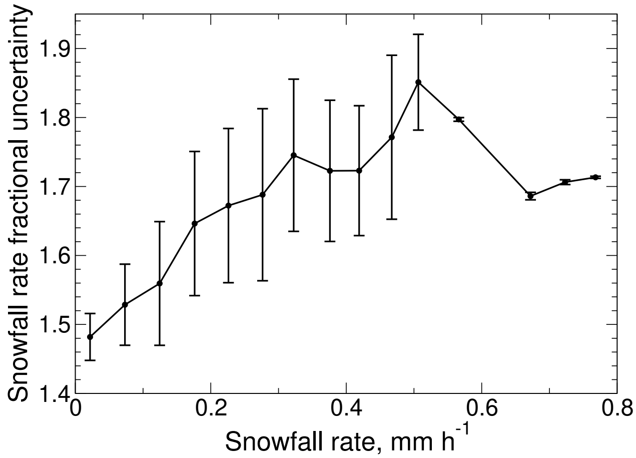

Figure 10. Instantaneous fractional uncertainties in snowfall rate. The central line shows mean fractional uncertainties and the error bars show +/- 1 standard deviation.

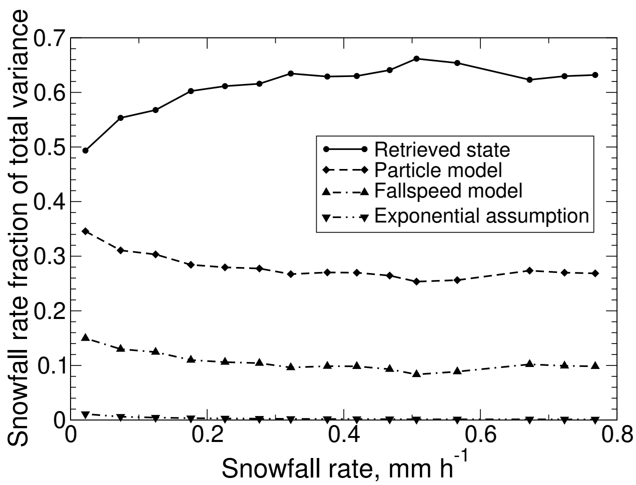

Figure 11. Instantaneous fractional variances for snowfall rate resolved by source.

4.2 Information content

The optimal estimation results allow easy calculation of a number of metrics that quantify retrieval performance in terms of information content (Rodgers, 2000; Shannon and Weaver, 1949). These include the averaging kernel matrix

$$\mathbf{A} = \left(\hat{\mathbf{K}}^{\mathsf{T}}\mathbf{S}_{\epsilon}^{-1}\hat{\mathbf{K}} + \mathbf{S}_{a}^{-1}\right)^{-1}\hat{\mathbf{K}}^{\mathsf{T}}\mathbf{S}_{\epsilon}^{-1}\hat{\mathbf{K}}, \tag{22}$$

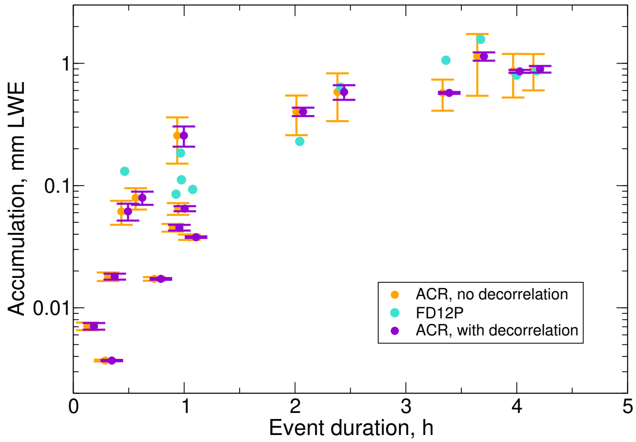

Figure 12. End-of-event accumulations and uncertainties. The P_{ACR} accumulation uncertainties are estimated assuming intra-event errors are perfectly correlated (orange) and decorrelated using a negative exponential model with a decorrelation scale of 0.5 hours (purple). P_{FD12P} accumulations (~~black~~blue-green) are shown for comparison except for those equal to zero which are omitted. For clarity, the P_{ACR} accumulations are plotted at +/- 0.02 hours (purple/orange) of their actual durations.

the Shannon Information Content

$$H = \frac{1}{2}\log_2 \left|\mathbf{S}_a \hat{\mathbf{S}}_x^{-1}\right|, \tag{23}$$

and the degrees of freedom for signal

$$d_S = \mathrm{Tr}\left(\mathbf{A}\right). \tag{24}$$

Briefly, the diagonal values of $\mathbf{A}$ indicate the degree to which the corresponding retrieved state variables are determined by the observations (values nearer 1) versus the a priori (values nearer 0). H measures how well the observations serve to narrow the possible retrieved states in comparison to the a priori. Its value can be interpreted as describing the binary bits of resolution of the observing system (L'Ecuyer et al., 2006). d_S quantifies the number of independent quantities that are determined by the observations. See Rodgers (2000) for a more complete discussion in the context of retrieval theory.

For the ACR retrievals, values for H vary between 0.4 and 1.2 (Fig. 13), indicating that the measurements resolve between 1.3 and 2.3 distinct states. Values for d_s show that the retrieval produces somewhat less than one independent piece of information that is significant compared to the measurement and forward model uncertainties. The lower two panels of Figure 13 show the diagonal elements of $\mathbf{A}$. While the element relevant to λ, $\mathbf{A}\left[\log\left(\lambda\right)\right]$, is consistently positive, the element for N_o , $\mathbf{A}\left[\log\left(N_0\right)\right]$ is near zero and is at times negative. These results show that $\log\left(\lambda\right)$ is moderately to strongly constrained by the reflectivity observation, while $\log\left(N_0\right)$ is largely dependent on the a priori constraint.

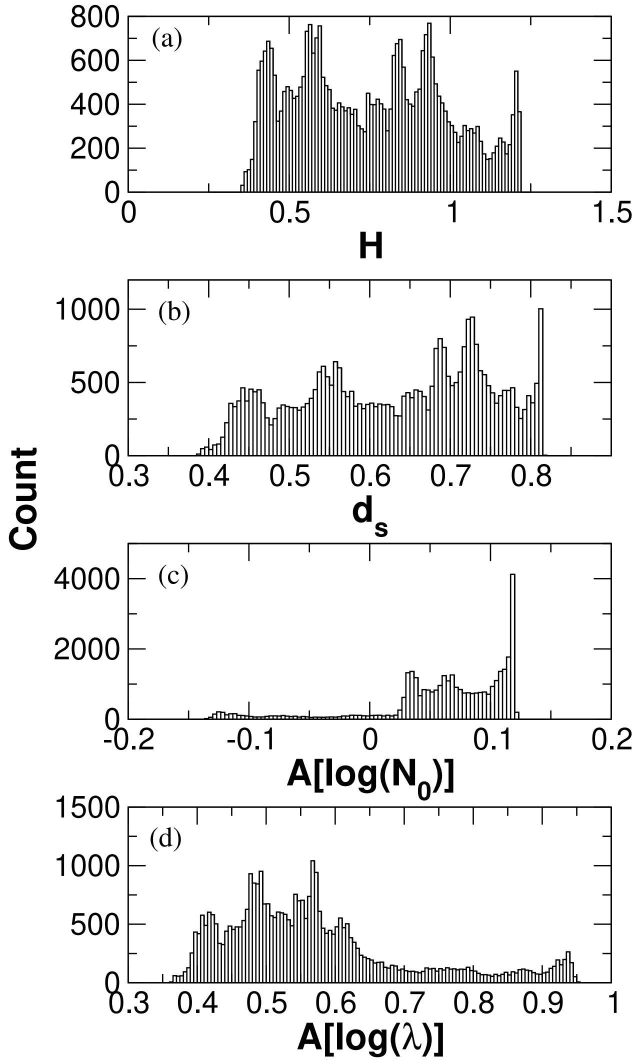

Figure 13. Distributions of information content metrics for the ACR retrieval.

The ~~shape of the~~ size distribution plays a significant role in determining the values of these metrics. Information content H increases as the distribution narrows (Fig. 14, panel a). The increase in H accompanies a substantial increase in the magnitude of the sensitivity of the forward model to $\log(\lambda)$ (panel b). In contrast, the sensitivity to $\log(N_0)$ has a constant value of 10 owing to the reflectivity in $\mathrm{dBZ_e}$ being a linear function of $\log(N_0)$ (and so is not shown in Figure 14). This increased sensitivity to $\log(\lambda)$ allows the observed reflectivity to better constrain the retrieved state, particularly the value of $\log(\lambda)$. As a result, $\mathbf{A}[\log(\lambda)]$ increases from 0.4 to 0.95 as λ increases (panel c). The behavior of $\mathbf{A}[\log(N_0)]$ (panel d) is quite different. The values are small and are positive for small values of λ, but become negative as λ increases. This behavior results from the positive a priori correlation between $\log(\lambda)$ and $\log(N_0)$, and the opposing signs of the sensitivities of $\mathrm{dBZ_e}$ to these two

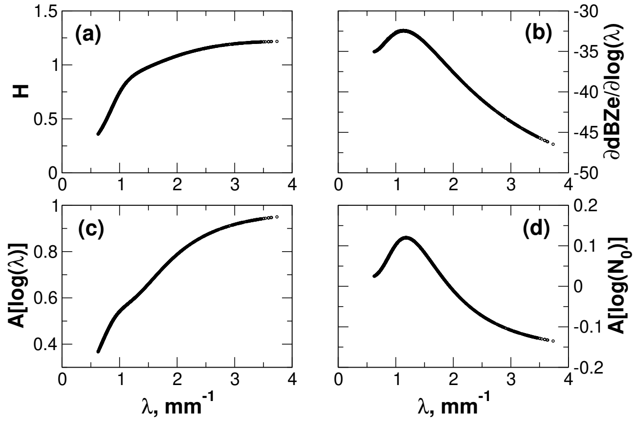

Figure 14. Information content metrics and the forward model Jacobian as functions of λ.

variables. While the forward model is strongly sensitive to $\log(\lambda)$, its sensitivity to $\log(N_0)$ is 3-4 times smaller in magnitude. ~~This sensitivity has a constant value of 10 owing to the reflectivity in $\mathrm{dBZ_e}$ being a linear function of $\log(N_0)$.~~ Consequently, the retrieved value of $\log(\lambda)$ is influenced more strongly by the observations, while the retrieved value of $\log(N_0)$ is influenced more by the a priori estimate of the state. This difference is reflected in panels (c) and (d) of Figure 14.

5 Discussion and conclusions

While millimeter-wavelength, single-frequency radar reflectivity observations alone would seem to have limited utility for retrieving snowfall properties, the results herein demonstrate capabilities for quantifying snowfall rate, accumulation and aspects of the snow PSD. The results were obtained by applying the radar observations to constrain a priori information appropriate to a broad range of snowfall regimes. The results indicate that the approach would provide useful information when applied to observations such as those from satellite-borne radars, which observe a range of snowfall regimes and for which radar observables are limited to reflectivity.

The results demonstrate the ability of the retrieval to produce reliable estimates of snow accumulation, particularly over time scales involving multiple events and more than several hours of snowfall duration, in spite of large uncertainties in retrieved instantaneous snowfall rates. For the C3VP season, the retrieval reproduced the observed accumulation within 13% at the end of the season. These results were achieved by omitting two particular time periods during which the retrieval's ~~dry snow assumptions were~~ particle property assumptions were likely very inconsistent with the observed snowfall. Without this adjustment, the end-of-season absolute difference was 18.9%, illustrating the need for adequate discrimination of the precipitation phase in the retrieval process. Keeping in mind that certain a priori assumptions of the retrieval were also sourced from the C3VP observations, these results are probably best viewed as indicating proper function of the retrieval. The time series of seasonal accumulation shows that while the initial fractional differences reach almost 80%, the differences diminish with time and increasing accumulation, reaching values of less than 5% within five hours. ~~For~~ These results are partly due to offsetting errors between events; however, for individual events, best agreement between the observed and retrieved snow accumulations were achieved for events that were longer in duration and produced more substantial accumulations. The observed accumulations for these events were mostly near or within the tighter uncertainty bounds produced by a decorrelating error model applied to the retrieved accumulation. The modest decorrelation used in the model produces uncertainties in the retrieved event accumulations of only 1% to 20%. Thus despite large instantaneous snowfall rate uncertainties for these single-frequency, millimeter-wavelength retrievals, retrieved rates can be expected to prove of value for quantifiying accumulations over events, months, seasons, and longer.

Uncertainties in instantaneous retrieval-estimated snowfall rate are dominated by uncertainties in the retrieved state (the uncertainties in the estimated PSD), followed by uncertainties in particle model parameters and to a lesser extent, the uncertainties in the fallspeed model. Uncertainties due to the assumption of an exponential PSD form are negligible. There is a degree of ambiguity here. The uncertainties in the particle model parameters contribute to the uncertainties in the estimated snowfall rate due to the appearance of the mass term in Eq. (18) but also contribute to uncertainties in the retrieved state. We treat these as independent contributions to the uncertainty. There is likely some covariance that could reduce total uncertainties but this is not addressed in the treatment of snowfall rate uncertainty presented here.

Retrieval performance, quantified in terms of information content metrics, is determined by the sensitivity of the observations to the desired state vector, the uncertainties assessed for the forward models and measurements, and the explicit assumptions about the uncertainty in the a priori knowledge of the state. For W-band modeled reflectivities in dB, the magnitude of sensitivities for $\log(\lambda)$ are 3-4 times those for $\log(N_0)$, and sensitivities are opposite in sign. This contributes to $\log(\lambda)$ being better constrained by the retrieval than is $\log(N_0)$. The consequences of these sensitivities are described more fully in Appendix A. To the extent that process information can be gleaned from changes in the slope parameter over time or space, the retrieval may be useful for process analyses when more direct observations of PSD are not available.

Model-measurement uncertainties are dominated by uncertainties in the particle model parameters (e.g., the coefficients and exponents of the mass- and area-dimension relationships, Table 2), and it is the uncertainties in mass parameters that are the most substantial contributor (Wood et al., 2015). For these near-surface observations, contributions to uncertainties in W-band radar reflectivity from shape, the assumption of an exponential form for the PSD, and the discrete-truncated form of the integrations over size distribution were not significant. For longer wavelength radars that might be used in similar applications (e. g., the MRR or KAZR), shape uncertainty will likely be even smaller due to less prevalent non-Rayleigh scattering.

These baseline results suggest several avenues for improving such single-frequency, radar reflectivity-based snowfall retrievals. Improved constraints on snow PSD parameters, through either reduced a priori uncertainties or better observational constraints, are paramount. For ground- or aircraft-based observations, ancillary measurements of snow PSDs can improve the a priori constraints. For retrievals from satellite-borne radar where such measurements are not available, the a priori state is given by more broadly applicable relationships for PSD parameters like those presented here. To the extent that a priori states for specific snowfall regimes might have smaller uncertainties, knowledge of regime-specific PDFs for snow PSD parameters would improve retrieval results provided the correct regime can be diagnosed by the retrieval. Coincident dual-frequency radar observations may also provide improved constraints on the snow PSD parameters (Liao et al., 2005; Matrosov, 2011) but

Table 2. Contributions to uncertainties in forward-modeled and observed reflectivity.

Source	Reflectivity, dB
Observed reflectivity	< 0.5
Particle model	5. - 15.
Shape	2.
Assumed exponential	< 1.
Truncation	0.42
Discretization	0.
Random dipole locations	0.

among current satellite-borne instruments, the CPR is single-frequency, and while the GPM DPR provides dual-frequency observations, the DPR sensitivities limit observations to heavier snowfall (Skofronick-Jackson et al., 2019) and implementation of dual-frequency snowfall retrieval has proven difficult (Iguchi et al., 2018). Finally, model-measurement uncertainties can be reduced by reducing uncertainties in particle mass estimates. This may require a more synergistic approach in which improved PSD information is coupled with additional observations such as Doppler velocity to better constrain the assumed particle model used in the retrieval, e.g., moving toward the approach used by Wood et al. (2014, 2015) with ground-based observations. The methods presented here, easily adaptable to other observing systems providing multiple frequency or collocated Doppler velocity observations, provide the basis from which such improvements can be tested and evaluated.

Data availability. Data used in this study can be obtained from the NASA Global Hydrology Resource Center's Distributed Active Archive Center at https://ghrc.nsstc.nasa.gov under DOIs TBD.

Appendix A: Retrieval interpretation

To interpret the behavior of the retrieval, we refer to the discussion of the information content metrics (Section 4.2). The small values for $\mathbf{A}\left[\log\left(N_0\right)\right]$ indicate its value is determined primarily by the a priori information and the negative signs do not fit the normal paradigm used to explain the $\mathbf{A}$ matrix. Their explanation reveals details of the significant behavior of this retrieval. In the application of the retrieval to a single radar bin, the value of $\mathbf{A}\left[\log\left(N_0\right)\right]$ is given by

$$\begin{aligned}\mathbf{A}\left[\log\left(N_0\right)\right] \quad = \quad & \left[s^2\left(\log\left(\hat{N}_0\right)\right)\left(\frac{\partial dBZe}{\partial \log\left(N_0\right)}\right)^2 + \right. \\ & \left. s\left(\log\left(\hat{N}_0\right), \log\left(\hat{\lambda}\right)\right)\left(\frac{\partial dBZe}{\partial \log\left(N_0\right)}\right)\left(\frac{\partial dBZe}{\partial \log\left(\lambda\right)}\right)\right]\left[s_y^2\left(dBZe\right)\right]^{-1},\end{aligned} \tag{A1}$$

where the carets indicate retrieved values. In the first set of brackets on the right side, the sign of the first term is clearly positive, while that of the second term depends on the signs of the covariance and the two partial derivatives, which are the elements of the Jacobian of the forward model. As was shown earlier (Fig. 14), $\frac{\partial dBZe}{\partial \log(N_0)}$ is positive while $\frac{\partial dBZe}{\partial \log(\lambda)}$ is negative. The covariance for the retrieved state changes very little from the a priori covariance, which is positive and represents a substantial correlation between $\log(\lambda)$ and $\log(N_0)$. This second term, then, is negative and as the magnitude of $\frac{\partial dBZe}{\partial \log(\lambda)}$ increases, the sign of $\mathbf{A}[\log(N_0)]$ changes from positive to negative.

These terms represent competing influences on the retrieved value of $\log(N_0)$. These competing influences arise from the a priori covariance and from the Jacobian of the forward model. The positive covariance requires that a positive adjustment in $\log(\lambda)$ be accompanied by a positive adjustment in $\log(N_0)$. In contrast, the Jacobian terms have differing signs. If the difference between the observed and forward model reflectivity calls for a positive adjustment to $\log(\lambda)$, the corresponding adjustment to $\log(N_0)$ would be negative.

Figure A1 shows this process schematically. The size distribution that represents the initial state is shown by the solid line. Assuming that the forward modeled reflectivity for this state overestimates the observed reflectivity (a positive error), two responses are possible: $\log(\lambda)$ could be increased, narrowing the distribution; and $\log(N_0)$ could be decreased, reducing the amplitude of the distribution. Absent the covariance between $\log(\lambda)$ and $\log(N_0)$, the retrieval would apply both adjustments, likely giving more weight to the adjustment of $\log(\lambda)$ because of the stronger sensitivity of the forward model to that variable. These adjustments are represented by the heavy arrows labeled $\delta\log(N_0)$ and $\delta\log(\lambda)$. Because of the positive covariance between $\log(N_0)$ and $\log(\lambda)$, however, an increase in $\log(\lambda)$ produces an opposing response that increases $\log(N_0)$, shown by the upward-pointing heavy arrow. The resulting size distribution is shown by the dashed line.

For small λ (broad distributions), the magnitude of $\frac{\partial dBZe}{\partial \log(\lambda)}$ is relatively small, so the covariance-driven adjustment is small and does not overcome the initial reduction in $\log(N_0)$. In these cases, $\log(N_0)$ decreases in response to a positive error in the modeled reflectivity. This net response is consistent with the sensitivity of the forward model to $\log(N_0)$ and $\mathbf{A}[\log(N_0)]$ is positive. For large λ (narrower distributions), the magnitude of $\frac{\partial dBZe}{\partial \log(\lambda)}$ is larger. The covariance-driven adjustment is larger also and does overcome the initial reduction in $\log(N_0)$. As a result, $\log(N_0)$ increases in response to the positive error in the modeled reflectivity. Since this net response opposes the sensitivity of the forward model, $\mathbf{A}[\log(N_0)]$ is negative.

The combination of the strong positive covariance between $\log(N_0)$ and $\log(\lambda)$ and the comparatively weak sensitivity of the reflectivity to $\log(N_0)$ limits the behavior of the retrieval. For narrower distributions, the retrieval is prevented from simultaneously increasing $\log(\lambda)$ and decreasing $\log(N_0)$ in response to a positive error in reflectivity. The opposing behavior, decreasing $\log(\lambda)$ and increasing $\log(N_0)$ in response to a negative error in reflectivity, is also restricted. While correct in a climatological sense since $\log(\lambda)$ and $\log(N_0)$ are positively correlated, in nature there are likely scenes for which such responses would give a more accurate retrieval. This reasoning demonstrates how other measurements, specifically those with better sensitivity to $\log(N_0)$, would benefit the retrieval.

Appendix B: Particle model

The properties here are for the particle shape denoted as “B8pr-30” from Wood et al. (2015), an idealized 8-arm branched spatial particle. Values for the parameters of the mass- and area-dimension power functions are

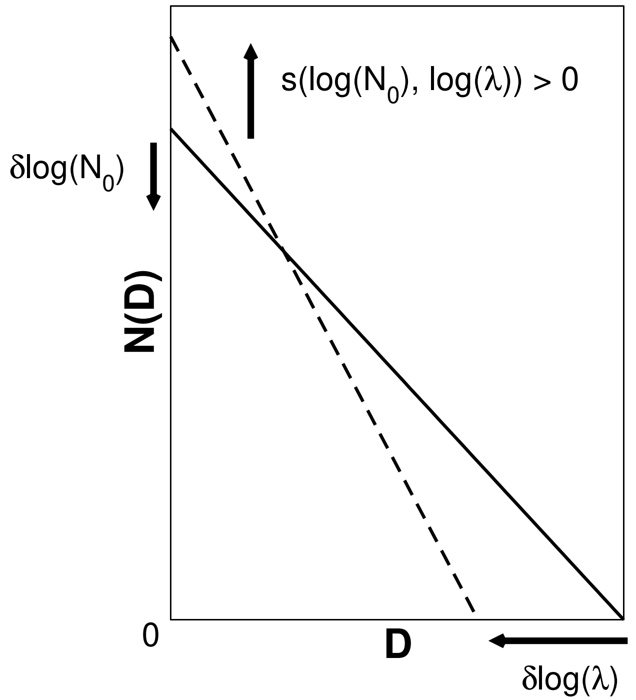

Figure A1. Schematic illustration of the retrieval process. The solid line represents the initial state of the retrieval while the dashed line shows the adjusted state assuming the initial state overestimates the observed reflectivity. The arrows labeled $\delta \log(\lambda)$ and $\delta \log(N_0)$ show the expected responses of the retrieval based on the sensitivities of the forward model. The arrow labeled $s(\log(N_o), \log(\lambda))$ shows the response due to positive covariance between λ and N_0.

$$\begin{aligned} \ln(\alpha) &= -5.723 \\ \beta &= 2.248 \\ \ln(\gamma) &= -1.379 \\ \sigma &= 1.813 \end{aligned}$$

with error covariance matrix

$$\mathbf{S}_b = \begin{matrix} 0.592 & 0.212 & 0.090 & 0.023 \\ 0.212 & 0.142 & 0.011 & 0.007 \\ 0.090 & 0.011 & 0.335 & 0.103 \\ 0.023 & 0.007 & 0.103 & 0.046 \end{matrix} .$$

Table B1. Backscatter and extinction properties for the snow particle model.

D_M mm	C_{bk} m^2	C_{ext} m^2	D_M mm	C_{bk} m^2	C_{ext} m^2
0.025	5.16253e-17	3.52024e-14	3.000	1.60708e-08	3.31323e-08
0.050	1.20475e-15	1.77890e-13	3.250	1.64139e-08	4.21088e-08
0.075	8.27182e-15	5.00664e-13	3.500	1.66119e-08	5.22600e-08
0.100	3.06847e-14	9.89618e-13	4.000	1.55864e-08	7.74061e-08
0.125	8.40498e-14	1.67138e-12	4.500	1.77554e-08	1.11609e-07
0.150	1.92314e-13	2.58903e-12	5.000	3.06798e-08	1.58860e-07
0.200	7.17250e-13	5.30976e-12	5.500	1.93705e-08	2.00667e-07
0.250	1.91396e-12	9.14038e-12	6.000	1.04092e-07	2.83080e-07
0.300	4.35436e-12	1.48681e-11	6.500	9.75512e-08	3.35067e-07
0.350	8.56280e-12	2.25304e-11	7.000	1.49787e-07	4.13047e-07
0.400	1.54761e-11	3.31046e-11	7.500	2.30734e-07	5.10512e-07
0.450	2.58963e-11	4.69409e-11	8.000	3.13418e-07	6.07034e-07
0.500	4.11161e-11	6.52071e-11	8.500	2.88081e-07	7.06213e-07
0.600	8.93929e-11	1.16523e-10	9.000	2.94080e-07	8.59293e-07
0.700	1.75650e-10	2.00793e-10	9.500	2.01596e-07	9.74101e-07
0.800	3.06043e-10	3.20526e-10	10.000	2.07686e-07	1.12076e-06
0.900	4.97542e-10	4.93081e-10	11.000	2.33291e-07	1.46061e-06
1.000	7.65231e-10	7.27755e-10	12.000	5.94999e-07	1.90676e-06
1.250	1.82454e-09	1.67311e-09	13.000	5.45403e-07	2.27318e-06
1.500	3.56830e-09	3.30096e-09	14.000	6.63279e-07	2.81244e-06
1.750	5.83188e-09	5.75812e-09	15.000	9.90939e-07	3.58772e-06
2.000	8.34684e-09	9.01675e-09	16.000	6.39329e-07	4.18269e-06
2.250	1.10293e-08	1.33794e-08	17.000	7.07551e-07	4.86569e-06
2.500	1.38623e-08	1.90102e-08	18.000	1.05353e-06	5.83543e-06
2.750	1.50482e-08	2.53761e-08			

These values are appropriate for use with particle size D_M in centimeters, mass in grams and area in square centimeters. The radar backscatter and extinction cross-sections are given in Table B1 versus particle size.

Data availability. Observational data used in this work are availabe as https://doi.org/xxxxx from the xxx-archive-name-xxx.

Author contributions. TSL and NBW developed the retrieval method from an initial concept by TSL. NBW performed the analyses and prepared the manuscript with contributions from TSL.

Competing interests. The authors declare that they have no conflict of interest.

Acknowledgements. Work by TSL and NBW was performed at University of Wisconsin - Madision and at Colorado State University for the Jet Propulsion Laboratory, California Institute of Technology, sponsored by the National Aeronautics and Space Administration. ~~The authors also acknowledge~~ We acknowledge our appreciation to Peter Rodriguez and David Hudak of Environment and Climate Change Canada for managing and making available C3VP observations used in this work. We thank Dr. Max Maahn and two anonymous reviewers for providing their feedback on this manuscript.

References

Austin, R. T., L'Ecuyer, T. S., and Seaman, C.: C3VP ACR operator's log. Unpublished manuscript, in possession of the author, 2007.

Bharadwaj, N., Lindenmaier, A., Widener, K. B., Johnson, K. L., and Venkatesh, V.: Ka-band ARM zenith profiling radar (KAZR) network for climate study. 36th Conf. on Radar Meteorology, Breckenridge, Colo., Am. Meteorol. Soc, 14A.8. [Available online at https://ams.confex.com/ams/36Radar/webprogram/Manuscript/Paper228620/14A8_ams_radconf_kazr.pdf, accessed 15 April 2020], 2013.

Boggs, P. T., Byrd, R. H., Rogers, J. E., and Schnabel, R. B.: User's reference guide for ODRPACK version 2.01 software for weighted orthogonal distance regression. U. S. Department of Commerce, National Institute of Standards and Technology, Applied Computational Mathematics Division, Gaithersburg, MD. NISTIR 92-4834. 99 pp, 1992.

Braham, Jr., R. R.: Snow particle spectra in lake effect snows. J. Appl. Meteorol., 29, 200-207, 1990.

Brandes, E. A., Ikeda, K., Zhang, G., Schoenhuber, M., and Rasmussen, R. M.: A statistical and physical description of hydrometeor distributions in Colorado snowstorms using a video disdrometer. J. Appl. Meteorol. Clim., 46, 634-650, doi:10:1175/JAM2489.1, 2007.

Chandrasekar, V., Joshil, S. S., Kumar, M., Vega, M. A., Wolff, D., and Petersen, W.: Snowfall observations during the Winter Olympics of 2018 campaign using the D3R radar. IGARSS 2019: 2019 IEEE International Geoscience and Remote Sensing Symposium, Yokohama, Japan, July 2019, 4561-4564, 2019.

Cooper, S. J., L'Ecuyer, T. S., Gabriel, P., Baran, A. J., and Stephens, G. L.: Objective assessment of the information content of visible and infrared radiance measurements for cloud microphysical property retrievals over the global oceans. Part II: Ice clouds. J. Appl. Meteorol. Clim., 45, 42-62, 2006

Draine, B. T., and Flatau, P. J.: Discrete-dipole approximation for scattering calculations. J. Opt. Soc. Am. A, 11, 1491-1499, 1994.

Goodison, B. E., Louie, P. Y. T., and Yang, D.: WMO solid precipitation measurement intercomparison: Final report. World Meteorological Organization Instruments and Observing Methods Report No. 67, WMO/TD - No. 872. 88pp plus 212 pp. Annexes, 1998.

Gordon, G. L., and Marwitz, J. D.: An airborne comparison of three PMS probes. J. Atmos. Ocean. Tech., 1, 22-27, 1984.

Gordon, G. L., and Marwitz, J. D.: Hydrometeor evolution in rainbands over the California valley. J. Atmos. Sci., 43, 1087-1100, 1986.

Gunn, K. L. S., and Marshall, J. S.: The distribution with size of aggregate snowflakes. J. Meteorol., 15, 452-461, 1958.

Herzegh, P. H., and Hobbs, P. V.: Size spectra of ice particles in frontal clouds: correlations between spectrum shape and cloud conditions. Q. J. Roy. Meteor. Soc., 111, 463-477, 1985.

Heymsfield, A. J.: Ice crystal terminal velocities. J. Atmos. Sci., 29, 1348-1357, 1972.

Heymsfield, A. J., and Miloshevich, L. M.: Parameterizations for the cross-sectional area and extinction of cirrus and stratiform ice cloud particles. J. Atmos. Sci., 60, 936-956, 2003.

Heymsfield, A. J., Field, P., and Bansemer, A.: Exponential size distributions for snow. J. Atmos. Sci., 65, 4017- 4031, doi:10.1175/2008JAS2583.1, 2008.

Houze, Jr., R. A., Hobbs, P. V., Herzegh, P. H., and Parsons, D. B.: Size distributions of precipitation particles in frontal clouds. J. Atmos. Sci., 36, 156-162, 1979.

House, Jr., R. A., and co-authors: The Olympic Mountains Experiment (OLYMPEX). Bull. Am. Meteorol. Soc., 98, 2167-2188, doi:10.1175/BAMS-D-16-0182.1, 2017

Hudak, D., Barker, H., Rodriguez, P., and Donovan, D.: The Canadian CloudSat validation project. Proc. Fourth European Conf. on Radar in Hydrology and Meteorology, Barcelona, Spain, 609-612, 2006. [Available online at http://www.crahi.upc.edu/ERAD2006/proceedingsMask/00165.pdf, downloaded 20 April 2020].

Iguchi, T., Kawamoto, N., and Oki, R.: Detection of intense ice precipitation with GPM/DPR. J. Atmos. Oceanic Technol., 35, 491-502, doi:10.1175/JTECH-D-17-0120.1, 2018.

Imai, I., Fujiwara, M., Ichimura, I., and Toyama, Y.: Radar reflectivity of falling snow. Papers in Meteorology and Geophysics, 6, 130-139, 1955.

Jones, E., and co-authors: SciPy: Open source scientific tools for Python. [Available online at \url{http://www.scipy.org}, accessed 24 Sep 2010], 2001.

Kajikawa, M.: Measurement of falling velocity of individual snow crystals. J. Meteorol. Soc. Jpn., 50, 577-584, 1972.

Kajikawa, M.: Measurements of falling velocity of individual graupel particles. J. Meteorol. Soc. Jpn., 53, 476-481, 1975.

Kajikawa, M.: Observations of the falling motion of early snow flakes. Part I: Relationship between the free-fall pattern and the number and shape of component snow crystals. J. Meteorol. Soc. Jpn., 60, 797-803, 1982.

Klugmann, D., Heinsohn, K., and Kirtzel, H. J.: A low cost 24 GHz FM-CW Doppler radar rain profiler. Contrib. Atmos. Phys., 61, 247-253, 1996.

Kulie, M. S., and Bennartz, R.: Utilizing spaceborne radars to retrieve dry snowfall. J. Appl. Meteorol. Clim., 48, 2564-2580, doi:10.1175/2009JAMC2193.1, 2009.

Liao, L., Meneghini, R., Iguchi, T., and Detwiler, A.: Use of dual-wavelength radar for snow parameter estimates. J. Atmos. Oceanic Technol., 22, 1494-1506, 2005.

L'Ecuyer, T. S., Gabriel, P., Leesman, K., Cooper, S. J., and Stephens, G. L.: Objective assessment of the information content of visible and infrared radiance measurements for cloud microphysical property retrievals over the global oceans. Part I: Liquid clouds. J. Appl. Meteorol. Clim., 45, 20-41, 2006.

Liu, G.: Deriving snow cloud characteristics from CloudSat observations. J. Geophys. Res., 113, D00A09, doi:10.1029/2007JD009766, 2008.

Lo, K. K., and Passarelli Jr., R. E.: The growth of snow in winter storms: An airborne observational study. J. Atmos. Sci., 39, 697-706, 1982.

Lobl, E. S., Aonashi, K., Griffith, B., Kummerow, C., Liu, G., Murakami, M., and Wilheit, T.: Wakasa Bay, an AMSR precipitation validation campaign. Bull. Am. Meteorol. Soc., 88, 551-558, 2007.

Locatelli, J. D., and Hobbs, P. V.: Fall speeds and masses of solid precipitation particles. J. Geophys. Res., 79, 2185-2197, 1974.

Maahn, M., Burgard, C., Crewell, S., Gorodetskaya, I. V., Kneifel, S., Lhermitte, S., Van Tricht, K., and van Lipzig, N. P. M.: How does the spaceborne radar blind zone affect derived surface snowfall statistics in polar regions? J. Geophys. Res. Atmos., 119, 13,6005-13,620, doi:10.1002/2014JD022079, 2014.

Marks, C. J., and Rodgers, C. D.: A retrieval method for atmospheric composition from limb emission measurements. J. Geophys. Res., 98, 14939-14953, 1993.

Mascio, J., and Mace, G. G.: Quantifying uncertainties in radar forward models through a comparison between CloudSat and SPartICus reflectivity factors. J. ~~Geophy~~Geophys. Res. Atmos., 122, 1665-1684, doi:10.1002/2016JD025183, 2017.

Matrosov, S. Y.: A dual-wavelength radar method to measure snowfall rates. J. Appl. Meteorol., 37, 1510-1521, 1998.

Matrosov, S. Y.: Modeling backscatter properties of snowfall at millimeter wavelengths. J. Atmos. Sci., 64, 1727-1736, doi:10.1175/JAS3904.1, 2007.

Matrosov, S. Y.: Feasibility of using radar differential Doppler velocity and dual-frequency ratio for sizing particles in thick ice clouds. J. Geophys. Res., 116, D17202, doi:10.1029/2011JD015857, 2011.

Matrosov, S. Y, Shupe, M. D., and Dialalova, I. V.: Snowfall retrievals using millimeter-wavelength cloud radars. J. Appl. Meteorol. Clim., 47, 769-777, doi:10.1175/2007JAMC1768.1, 2008.

Matrosov, S. Y., Campbell, C., Kingsmill, D., and Sukovich, E.: Assessing snowfall rates from X-band radar reflectivity measurements. J. Atmos. Oceanic Technol., 26, 2324-2339, doi:10.1175/2009JTECHA1238.1, 2009.

Mitchell, D. L.: Use of mass- and area-dimensional power laws for determining precipitation particle terminal velocities, J. Atmos. Sci., 53, 1710-1723, 1996.

Mitchell, D. L., and Heymsfield, A. J.: Refinements in the treatment of ice particle terminal velocities, highlighting aggregates. J. Atmos. Sci., 62, 1637-1644, 2005.

Mitchell, D. L., Zhang, R., and Pitter, R. L.: Mass-dimension relationships for ice particles and the influence of riming on snowfall rates. J. Appl. Meteorol., 29, 153-163, 1990.

Moran, K. P., Martner, B. E., Post, M. J., Kropfli, R. A., Welsh, D. C., and Widener, K. B.: An unattended cloud-profiling radar for use in climate research. Bull. Amer. Meteor. Soc., 79, 443-455, 1998.

Nakada, U., and Terada, Jr., T.: Simultaneous observations of the mass, falling velocity and form of individual snow crystals. J. Fac. Sci., Hokkaido Univ., Ser. 2, 1, 191-200, 1935.

Newman, A. J., Kucera, P. A., and Bliven, L. F.: Presenting the Snowflake Video Imager (SVI). J. Atmos. Oceanic Technol., 26, 167-179. doi:10.1175/2008JTECHA1148.1, 2009.

Passarelli Jr., , R. E.: Theorectical and observational study of snow-size spectra and snowflake aggregation efficiencies. J. Atmos. Sci., 35, 882-889, 1978.

Petersen, W. A., L'Ecuyer, T., and Moisseev, D.: The NASA CloudSat/GPM Light Precipitation Validation Experiment (LPVEx). Earth Observer, 23, 4-8, 2011.

Pettersen, C., Kulie, M. S., Bliven, L. F., Merrelli, A. J., Petersen, W. A., Wagner, T. J., Wolff, D. B., and Wood, N. B.: A composite analysis of snowfall modes from four winter seasons in Marquette, Michigan, 2020. J. Appl. Meteorol. Clim., 59, 103-124, doi:10.1175/JAMC-D-19-0099.1, 2020.

Posselt, D. J., Li, X., Tushaus, S. A., and Mecikalski, J. R.: Assimilation of dual-polarization radar observations in mixed- and ice-phase regions of convective storms: Information content and forward model errors. Mon. Wea. Rev., 143, 2611-2636, doi:10.1175/MWR-D-14-00347.1, 2015.

Rodgers, C.: Inverse methods for atmospheric sounding, World Scientific Publishing, Singapore. 240 pp, 2000.

Rogers, D. C.: The aggregation of natural ice crystals. M. S. thesis, University of Wyoming, Laramie, Wyoming, 91 pp, 1973.

Ryan, B. F.: On the global variation of precipitating layer clouds. Bull. Am. Meteorol. Soc., 77, 54-70, 1996.

Schirle, C. E., Cooper, S. J., Wolff, M. A., Pettersen, C., Wood, N. B., L'Ecuyer, T. S., Ilmo, T., and Nygård, K.: Estimation of snow microphysical properties at a mountainous site in Norway using combined radar and in situ microphysical observations. J. Appl. Meteorol. Clim., 58, 1137-1362, doi:10.1175/JAMC-D-18-0281.1, 2019.

Shannon, C. E., and Weaver, W.: The mathematical theory of communication, Univ. of Illinois Press, Urbana, Ill., 117 pp., 1949.

Skofronick-Jackson, G., and co-authors: Global Precipitation Measurement Cold season Precipitation Experiment (GCPEx): For measurement's sake, let it snow. Bull. Am. Meteorol. Soc., 96, 1719-1741, doi:10.1175/BAMS-D-13-00262.1, 2015.

Skofronick-Jackson, G., Kulie, M., Milani, L., Munchak, S. J., Wood, N. B., and Levizzani, V.: Satellite estimation of falling snow: A Global Precipitation Measurement (GPM) Core Observatory perspective. J. Appl. Meteorol. Clim., 58, 1429-1448, doi:10.1175/JAMC-D-18-1024.1, 2019.

Tanelli, S., Durden, S. L., Im, E., Pak, K. S., Reinke, D. G., Partain, P., Haynes, J. M., and Marchand, R. T.: CloudSat's cloud profiling radar after two years in orbit: Performance, calibration and processing. IEEE. T. Geosci. Remote, 46, 3560-3573,2008.

Taylor, J. R.: An introduction to error analysis, University Science Books, Sausalito, CA, 327 pp., 1997.

Toyoshima, K., Masunaga, H., and Furuzawa, F. A.: Early evaluation of Ku- and Ka-band sensitivities for the Global Precipitation Measurement (GPM) Dual-frequency Precipitation Radar (DPR). SOLA, 16, 6-11, doi:10.2151/sola.2020-002, 2015.

Vaisala Oyj: Weather sensor FD12P user's guide M210296en-A, Vaisala Oyj, Helsinki, 154 pp., 2002.

Wood, N. B.: Estimation of snow microphysical properties with application to millimeter-wavelength radar retrievals for snowfall rate. Ph.D. dissertation, Colorado State University, Fort Collins, Colorado, 248 pp. [Available from Colorado State University, Digital Collections, http://hdl.handle.net/10217/48170], 2011.

Wood, N. B., L'Ecuyer, T. S., Bliven, F. L., and Stephens, G. L.: Characterization of video disdrometer uncertainties and impacts on estimates of snowfall rate and radar reflectivity. Atmos. Meas. Tech., 6, 3635-3648, doi:10.5194/amt-6-3635-2013, 2013.

Wood, N. B., L'Ecuyer, T. S., Heymsfield, A. J., Stephens, G. L., Hudak, D. R., and Rodriguez, P.: Estimating snow microphysical properties using collocated multisensor observations. J. Geophys. Res. Atmos., 119, 8941-8961, dol:10.1002/2013JD021303, 2014.

Wood, N. B., L'Ecuyer, T. S., Heymsfield, A. J., and Stephens, G. L.: Microphysical constraints on millimeter-wavelength scattering properties of snow particles. J. Appl. Meteorol. Clim., 54, 909-931, doi:10.1175/JAMC-D-14-0137.1, 2015.

Woods, C. P., Stoelinga, M. T., and Locatelli, J. D.: Size spectra of snow particles measured in wintertime precipitation in the Pacific Northwest. J. Atmos. Sci., 65, 189-205, doi:10.1175/2007JAS2243.1, 2008.

Zikmunda, J., and Vali, G.: Fall patterns and fall velocities of rimed ice crystals. J. Atmos. Sci., 29, 1334-1347, 1972.

Zikmunda, J., and Vali, G.: Corrigendum. J. Atmos. Sci., 34, 1675, 1977.